Construction and Building Materials 438 (2024) 137166

Contents lists available at ScienceDirect

Construction and Building Materials

journal homepage: www.elsevier.com/locate/conbuildmat

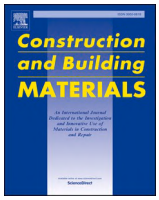

Employing limestone and calcined clay for preserving the strain-hardening response of PET fiber-reinforced cementitious composites

Ameer Hamza Ahmed , Cesare Signorini [*] , Mariam Chikhradze , Marco Liebscher , Marko Butler , Viktor Mechtcherine

Institute of Construction Materials, TU Dresden, Dresden 01062, Germany

A R T I C L E I N F O

Keywords:
PET
SHCC
LC^3
Alkaline environment
Mechanical performance
Multiple cracking

A B S T R A C T

The degradation of polyethylene terephthalate (PET) fibers in alkaline environments limits their use in strain-hardening cementitious composites (SHCC). Prolonged PET exposure to alkaline environments has a detrimental effect on its mechanical performance, mainly due to the physicochemical transformation caused by alkaline hydrolysis. This study presents a tailored cementitious matrix design containing high amounts of limestone and calcined clay, replacing 75 wt% of Portland cement, to attain and maintain the strain-hardening response of composites incorporating PET fibers as dispersed reinforcement. Analytical and mechanical tests were carried out at different curing ages, ranging from 7 to 60 days, to study the effects of aging on virgin PET fibers, both within the matrix and outside it (in the pore solution). The results showed a pronounced degradation of the PET fibers in the test pore solution at pH 12.5, manifested by a progressive reduction in the load-bearing capacity of the individual fibers with prolonged immersion. Conversely, when the PET fibers were aged in-matrix under laboratory conditions and tested under tension, the performance of the corresponding composites showed resilience to aging, exhibiting reasonable tensile strength and remarkable strain capacities that exceeded 4 %.

1. Introduction

Strain-hardening cementitious composites (SHCC), also known as engineered cementitious composites (ECC), were first developed in the 1990s to address many of the inherent limitations of traditional/reinforced concrete. These drawbacks include brittleness, poor crack control, bulky structural components, susceptibility to catastrophic failure under shear loading, *etc.* [1]. This category of advanced concrete composites incorporates discrete short polymer fibers as dispersed micro-reinforcements, typically added in a moderate volume content of about two percent. These fibers are randomly distributed in fine-grained brittle cementitious matrices. When subjected to tensile loading, after the formation of the first crack, these fibers act as crack-bridging agents, playing a pivotal role in transferring the applied load across the crack flanks and redistributing it back to the intact matrix through the phenomenon known as *"crack bridging"*. This leads to the scenario where the composite exhibits an increase in load-bearing capacity while undergoing large inelastic deformation, otherwise known as strain-hardening behavior [2]. This quasi-ductility stems from the formation of multiple parallel micro-cracks, entailing SHCC with remarkable energy absorption capabilities under quasi-static loading and, notably, under dynamic loading conditions, such as earthquakes, impacts, or blasts [3–5].

While designing SHCC, two critical criteria, guided by micromechanical principles, must be satisfied to achieve the strain-hardening behavior [1,6,7]. The first criterion, known as the *strength criterion*, is formulated to ensure that the tensile strength of the matrix is consistently outweighed by the bridging strength of the fibers in each crack plane. This condition prevents catastrophic failure in the composites, even if the matrix loses its integrity in a specific crack plane. The greater the disparity between the first crack stress and fiber bridging stress, the more pronounced the strain-hardening behavior is expected to be.

The second criterion, known as the *energy criterion*, regulates the steady-state crack propagation (flat crack, *i.e.,* constant crack tip opening displacement) and determines whether the bridging fibers undergo pull-out or rupture. This can be achieved by ensuring that the energy contribution from the bridging fibers is sufficiently higher than the toughness of the matrix at the crack tip itself. Detailed schematic illustrations and mathematical formulations for these two micromechanical criteria can be found in the work of V.C. Li [1], and can also be found

* Corresponding author.
E-mail address: cesare.signorini@tu-dresden.de (C. Signorini).

https://doi.org/10.1016/j.conbuildmat.2024.137166
Received 10 January 2024; Received in revised form 30 May 2024; Accepted 18 June 2024
Available online 26 June 2024

later in **Section 3.3.3** . Their fulfillment is substantially influenced by both the matrix design and the choice of dispersed fibers [8].

In general, high-performance fibers are well-suited for high-strength matrices, while low-strength and compliant fibers are more appropriate for low-strength matrices.

Synthetic polymeric fibers are typically the preferred choice for SHCC because of their high performance, durability, and widespread availability, setting them apart from natural and synthetic inorganic fibers [8]. Several polymeric fibers emerged as highly promising candidates for SHCC, each with distinct advantages and disadvantages [8]. Notable examples include polyvinyl alcohol (PVA), aramid, poly (p-phenylene-2,6-benzobisoxazole) (PBO), polypropylene (PP), and ultra-high molecular weight polyethylene (PE) [9–12], *cf.* Table 1. Among these synthetic fiber options, PVA and PE fibers have been extensively researched in the framework of the SHCC [5,13–19]. Their chemical stability renders them resistant to alkaline environments, typical in cementitious matrices. Furthermore, the strong interfacial bonds (*i.e.,* chemical and/or mechanical) between these fibers and high-strength cementitious matrices facilitate outstanding crack-bridging capabilities, thus enhancing the overall ductility of the composites. Nevertheless, the major downsides of using these fibers include the high cost, embodied energy, and CO_2 emissions associated with their production, ultimately undermining the final product's green credentials [8]. Furthermore, these fibers are embedded in high-strength, fine-grained cementitious matrices to unlock their full potential in improving the cost-to-performance ratio. This leads to significant reliance on Portland cement (PC), raising additional economic and environmental concerns [2].

A promising alternative is using polyethylene terephthalate (PET) fibers, which are thermoplastic polyesters commonly employed in plastic packaging. These fibers offer a means to address the cost of using PVA and PE fibers in SHCC. In fact, PET is the most synthesized fiber globally, accounting for 54 % of the market share of total fiber production [22], which pledges to its wide availability and, therefore, cost-effectiveness. The economic advantage is underscored by the considerably lower prices of PET fibers, which are 94 % and 54 % lower (by weight) than those of PE and PVA fibers, respectively, which were previously studied by Curosu *et al.,* [20]. Additionally, PET fibers are one of the most recycled polymers, with a recycling rate of approximately 15 % among other synthetic fibers [22], thereby augmenting the sustainability profile of PET-based products.

From both mechanical properties and durability perspectives, it's worth noting that PET fibers' tensile strength and stiffness are comparatively lower than those of PVA and PE fibers. In contrast, PET fibers exhibit a substantially higher fiber elongation, approximately ~34 %, compared to 6 % and 3.5 % for PVA and PE fibers, respectively [20,23]. As a common feature of polyesters, PET fibers are intrinsically hydrophobic owing to their limited moisture-absorption capability. Consequently, these fibers primarily form mechanical bonds with cementitious bodies, while adding them to a fresh concrete mixture has minimal impact on hydration [24]. Nevertheless, PET's long-term performance and stability in alkaline environments remain disputed, as in cementitious matrices. Some researchers have emphasized the sufficient alkaline resistance of PET fibers (*e.g.,* [25–28]), which has inspired others to use virgin and recycled PET fibers in concrete [29–34]. However, several other studies have highlighted the steadily deteriorating performance of PET fibers in alkaline environments. For instance, Wang *et al.,* [35] reported a significant reduction in the tensile strength of PET fibers in cementitious pastes. Similarly, Won *et al.,* [36] exposed PET fiber-reinforced composites to various aggressive environments and observed the progressive disintegration of the PET fiber surface when exposed to an alkaline environment. Studies conducted by Silva *et al.,* [37], Fernández *et al.,* [38], and Rostami *et al.,* [39] also provided evidence supporting the instability of PET fibers in cementitious systems. This deterioration is ascribed to the alkaline hydrolysis of PET, which converts ester groups into the corresponding carboxylic acids and alcohols. This phenomenon is accompanied by a loss of molecular weight due to polymer chain cutting, seen as pitting on the fiber surface, and a reduction in the diameter and strength of the fiber [24,40].

Conceivably, this is why only a handful of previous research studies have focused on using PET fibers in the context of SHCC. Yu *et al.,* [41] explored the potential of partially replacing PVA fibers with recycled PET fibers to reduce the cost and improve the sustainability of SHCC. Through micromechanical modeling and experimental findings, they achieved a 50 vol% replacement of PVA fibers with treated recycled PET fibers (investigated by Lin *et al.,* [42]) resulting in hybrid fiber SHCC with a tensile strain capacity of 2 % and tensile strength of 3.6 MPa. This hybrid approach reduced the embodied energy and material costs of the SHCC by 20 % and 40 %, respectively. However, multiple cracking or strain hardening was not observed when untreated virgin fibers were used alone. Further development of the same hybrid SHCC composites was carried out by Lu *et al.,* [43], where they focused on performance enhancement through matrix modification. Their work incorporated local (cost-effective) PVA and PET fibers into the matrix and a substantial amount of fly ash as a PC substitute. Although the positive effects of reducing PC on the tensile strain capacity of the PVA/PET hybrid SHCC were evident, no strain hardening was discerned when PET fibers were embedded in the matrix alone.

The substantial disparity in the mechanical properties of PVA and PET fibers complicates the achievement of strain-hardening behavior, especially when compliant PET fibers are incorporated into the matrix designed for PVA fibers. In PVA-SHCC, meeting the strength and energy criteria is relatively straightforward, thanks to the fiber's adequate elastic modulus, tensile strength, and good bonding affinity with the surrounding matrix. Conversely, in PET-SHCC, while the energy criterion can be met due to the high plastic deformation of PET fibers, the strength criterion often becomes the limiting factor [44]. The same is true for the matrices made solely of PC, which tend to have higher strength than blended cementitious systems with high PC replacement levels. Not to mention, the high alkalinity levels in pure PC-based matrices can affect the stability of PET fibers. Therefore, based on the aforementioned considerations, this study introduces a specially tailored cementitious matrix design for PET fibers inspired by a prior work conducted by the authors [45]. The design involves the incorporation of substantial quantities of limestone and calcined clay in lieu of 75 wt% of PC content to achieve the following conditions: (i) reducing the alkalinity of the matrix due to the limited contribution of alkali and hydroxides from the cement; (ii) limiting the mechanical strength of the matrix to facilitate strain-hardening behavior with PET fibers; and (iii) stabilizing the mechanical properties after a certain age due to limited clinker and portlandite content [45].

A comprehensive experimental program was conducted to prioritize two aspects: (i) out-of-matrix aging of virgin PET fibers in a simulated alkaline pore solution made from the novel matrix binder composition and (ii) in-matrix aging. The first part of the program is intended to explicitly ascertain the degradation potential of PET fibers by immersing

Table 1
Mechanical properties of some notable synthetic polymer fibers used in SHCC.

Fibers	σ_T [MPa]	ε_u [%]	E [GPa]	Remarks	Reference
PE	2500	3.5	80	High performance	[20]
PVA	1600	6.0	40	High performance	[20]
PBO-AS	5800	3.5	180	High performance	[10]
PBO-HM	5800	2.5	270	High performance	[10]
Aramid	3400	4.5	74	High performance	[10]
High-tenacity PP	928	7.3–30	11.6	Low performance	[8,21]

them in a simulated pore solution of pH 12.5 for 7, 14, 28, and 60 days and performing single fiber tension tests coupled with ESEM analysis for quantitative and qualitative assessment. The second part of the program consists of experiments at the composite level. Compression, single fiber pull-out, and uniaxial tension tests were performed at identical ages, *i.e.,* 7, 14, 28, and 60 days. In the end, some key conclusions were drawn from these results, and further improvements were suggested to promote PET fibers as cost-effective and sustainable alternative fibers in SHCC.

2. Materials and methods

2.1. Raw materials

Commercially available raw materials were employed to investigate the aging performance of PET fibers in both a cementitious matrix (in-matrix) and the pore solution (out-of-matrix). The high early strength, rapid setting, and sulfate-resistant Portland cement, CEM I 52.5 R-SR3/NA, was supplied by Holcim GmbH, Lägerdorf, Germany. Low-grade industrially calcined kaolinitic clay with a pre-calcination kaolinitic content limited to $\leq$ 25 %, along with several clay impurities [46], was acquired from Liapor GmbH & Co. KG, Hallendorf, Germany. The post-calcination amorphous content of the clay was approximately 65.7 %. Limestone powder (Saxodol 90 LE), with a total carbonate content of 98 % (54 % calcite plus 44 % dolomite), was sourced from sh minerals GmbH, Heidenheim/Brenz, Germany. High-purity gypsum was supplied by Grüssing GmbH, Germany.

These raw materials were utilized to formulate the binder composition of the blended cementitious matrix and pore solution. Additionally, fine quartz sand from Strobel Quarzsand, Germany, featuring a particle size range of 60–200 μm, was added as a fine inert aggregate to complete the cementitious matrix.

To enhance the fresh mix's workability and facilitate the uniform dispersion of the PET fibers, a viscosity-modifying agent (VMA, Unterwasser-Compound 100) from Sika® (Switzerland) and a polycarboxylate (PCE)-based superplasticizer (MasterGlenium ACE 460) from Master Builders Solutions (Germany) were incorporated into the mix design. The authors have published detailed information on these raw materials' chemical and mineralogical compositions and particle size distributions [45,47,48].

The PET fibers used in this study were provided by ADVANSA GmbH, Germany. For the single fiber pull-out specimens (discussed in more detail in Sections 2.4.2), 6 mm long chopped fibers were incorporated into the matrix composition. In comparison, longer 18 mm chopped fibers were used to prepare the SHCC specimens. In addition, long PET fibers were cut from the tow for the single-fiber tensile and pull-out tests. Table 2, the manufacturer's datasheet, details these fibers' physical and mechanical properties [23].

Table 2
Physical and mechanical properties of PET fibers as per manufacturer's datasheet [23]. Values in parentheses were measured by the authors.

Fibers	PET
Manufacturer, country	ADVANSA, Germany
Brand name	ADVA® Shortcut[a], ADVA®Tow[b]
Length (mm)	6[a], 18[a], long tow[b]
Diameter (μm)	18, (17 ± 0.69)
Tensile strength (MPa)	N.A, (584.8 ± 34.8)
Young's modulus (GPa)	N.A, (12.3 ± 6.9)
Fiber elongation (%)	34, (31.8 ± 3.3)
Density (g/cm^3)	1.37
Color	Semi-dull white
Melting point (°C)	~250

[a] 6 mm fibers were used in the matrix block of the single fiber pull-out specimens, whereas 18 mm fibers were used in the SHCC specimens for compression and uniaxial tensile tests.

[b] A few meters of tow were used to cut the fibers to the desired lengths for single-fiber tension tests.

2.2. Mixture design

In accordance with the objectives outlined earlier, the authors developed a specialized matrix design influenced by their prior research. Several strategic considerations were considered:

- A significant proportion of the PC was replaced by limestone and calcined clay (75 wt%), effectively limiting the alkali oxide content from the cement clinker and reducing the matrix's alkalinity. This significant reduction in clinker content inevitably led to a decrease in matrix strength, thus affecting the fiber/matrix interface properties, both of which were considered essential for inducing strain hardening using PET fibers.
- The water/binder ratio was set at 0.4, which is typically higher than conventional SHCC mix designs. This, in turn, resulted in increased porosity, which promoted the initiation of cracking within the matrix. In addition, given the low clinker content in the mix, the dilution effects accelerated the hydration of the clinker, achieving full hydration in a short time (a matter of a few days) [49,50]. Consequently, the amount of portlandite was also limited by the low clinker content in the matrix, which limited the pozzolanic reaction. This ensured that the mechanical strength of the matrix would stabilize after a certain hydration time, as all hydratable materials in the matrix were either consumed or depleted [45]. In addition, the increased water/binder ratio addressed the high water demand associated with calcined clay due to its larger specific surface area, improving workability and facilitating fiber dispersion in fresh mixes.
- A moderate volume fraction of PET fiber (2.5 %) was used to ensure an adequate level of crack-bridging stresses conducive to strain-hardening behavior. This fraction was higher than that typically used for stiffer fibers (2 vol%, such as PE/PVA). In addition, an appropriate aspect ratio of 1059, denoting the length-to-diameter ratio of the PET fibers (as shown in Table 2), was chosen to allow effective fiber anchorage in the crack flanks, thereby enhancing the crack-bridging capability of the composite.
- A low sand/binder ratio (s/b) of 0.23 was adopted to reduce the matrix's fracture toughness and promote crack propagation [51].

Table 3 presents the formulation of the SHCC matrix studied in this research, herein designated as Strain-Hardening Limestone Calcined Clay Cementitious Composite (abbreviated as SH-LC^3). The mix design incorporates a small amount of gypsum (3 wt% of the binder) for sulfate balance. In addition, superplasticizer and VMA were added to the mix to improve fiber dispersion and workability. The mixing procedure followed a similar protocol as previously described in the reference [48]; a standard protocol opted, in general, for SHCC.

2.3. Simulated pore solution preparation

While various methods exist for extracting real pore solutions from cementitious systems, such as vacuum filtration or centrifugation

Table 3
Mixture composition for the SH-LC^3. The quantities are listed in kg/m^3.

Mix constituents	Amount
Portland cement	286
Limestone	282
Calcined clay	564
Gypsum	9
Quartz sand	257
Fibers	34 (2.5 vol%)
Water	458
Superplasticizer	8
VMA	4

(typically during the initial hours of hydration) [52,53] or high-pressure devices following the hardening phase [54,55], the primary objective of this study is to explore the effects of a certain level of alkalinity on PET fibers, primarily expected within the matrix. The intention is not to analyze the actual pore solution.

Hence, a simulated pore solution was meticulously prepared. This involved blending 2.5 kg of the binder composition, which maintained the same proportions as the matrix formulation (consisting of PC, limestone, calcined clay, and gypsum, as detailed in Table 3), with 13 liters of tap water. This highly diluted mixture was subjected to intermittent mixing using a hand mixer for 2 minutes every 2 hours over a total duration of 8 hours. Subsequently, the container was sealed and allowed to stand overnight. The test pore water was filtered and transferred to sealed containers the following day. The pH of the test pore solution was measured immediately after collection and again at 7, 14, 28, and 60 days. This measurement was carried out using a digital pH meter equipped with an electrode, calibrated to pH values of 4, 7, and 10 using standard solutions. The average pH of the simulated solution was found to be 12.5 ± 0.1. This value is lower than the pH of actual pore solutions extracted from PC systems with a water/cement ratio of 0.4, which typically falls within the range of 13.6 [56]. The variance can be attributed to the diminished alkali oxides resulting from the lower cement content and the high dilution applied to the simulated pore solution [56,57].

2.4. Sample preparation and testing setups

2.4.1. Single fiber tension test

Single fiber tension tests were performed to evaluate the mechanical properties of PET fibers after aging them for 7, 14, 28, and 60 days within the formulated alkaline pore solution, all at room temperature. As a reference, as-received PET fibers were also tested. Following the designated immersion periods, the fibers were extracted from the test pore solution, thoroughly rinsed with distilled water, and subsequently dried in a climatic chamber set at 65 % relative humidity and 20°C for 24 hours.

The next step involved attaching single fibers onto a paper frame featuring a rectangular opening of 6 mm in the center that defined their free length. Cyanoacrylate adhesive anchors the fibers onto the paper frame at the upper and lower ends. These paper frames were then securely clamped on both sides using the Zwick/Roell 1445 machine, as depicted in Fig. 1 (a), with a zoomed view in the inlet (b). Subsequently, the frames were transversely cut at both sides to release the individual fibers. The tests were carried out using a 10 N load cell with an accuracy of ± 0.05 % under a constant displacement-controlled regime, maintaining a rate of 0.05 mm/s.

Before the tests, Environmental Scanning Electron Microscopy (ESEM) was performed on a minimum of 30 fibers to ascertain the diameter of both the reference and exposed fibers. The latter group was expected to display changes due to alkaline hydrolysis. The results were analyzed by determining the tensile stress-strain properties of PET, employing force-displacement data and cross-sectional areas of the fibers.

2.4.2. Single fiber pull-out test

To evaluate the interfacial properties between PET fibers and the SH-LC^3 matrix, single-fiber pull-out tests were conducted at the corresponding curing durations, matching those of the single fibers immersed in the pore solution (7, 14, 28, and 60 days). Despite the differences in curing conditions between in-matrix aging (sealed curing under laboratory conditions) and out-of-matrix aging (immersion in the pore solution), it was expected that the initial wetting of the PET fibers in the fresh SH-LC^3 slurry, along with the sustained high relative humidity due to sealing, would initiate hydrolysis. To ensure the reproducibility of our methods, readers are referred to the sample preparation protocol previously described in a study [20], which was strictly adhered to in this research.

A slender beam 4 mm thick, defining the fiber embedment length, was cast around the individual PET fibers using a fiber-reinforced matrix containing 2 % by volume of 6 mm long PET fibers. The PET fibers' reduced volume fraction and aspect ratio compared to the compression and uniaxial tension test specimens were chosen to facilitate the matrix casting in the 4 mm wide notches of the molds. Embedding the fibers in the matrix block of the pull-out specimens minimized matrix spalling during pull-out, thereby providing a more accurate assessment of bond strength [20].

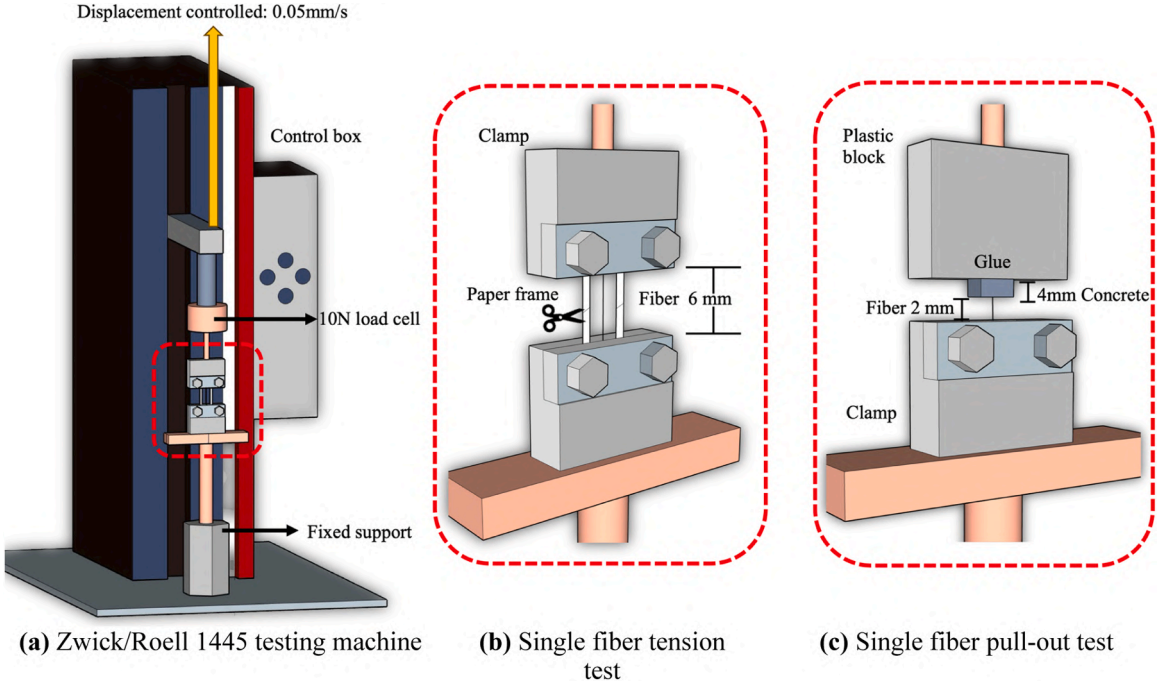

Fig. 1. Schematics of the testing device – Zwick/Roell 1445 (a); for single fiber tension test (b); and single fiber pull-out test (c).

Before sealing the specimens in plastic bags for curing for defined periods of time, the inside of the bags was moistened to maintain a high humidity level. The sealed specimens were then stored in a climate chamber at a controlled temperature of 20 ± 2 °C. One day before testing, the beams were dry-cut into small cubic blocks of 4 × 4 × 4 mm^3, with a single fiber protruding from the center for secure anchorage during the pull-out experiments. A small paper frame was used for fiber attachment at the free end. The tests were performed on the same Zwick/Roell 1445 testing machine. In contrast to the clamps at both ends used in the fiber tensile test, a plastic block was used at the top, with the concrete block attached using a high-speed UV adhesive (cure time of 10–15 seconds under UV light). Fig. 1 (c) shows a schematic of the test setup. The test parameters, namely load cell and displacement rate, remained the same as those used in the single fiber tensile test.

With the help of the obtained force-displacement curves, the frictional bond (τ), chemical bond (G_d), and pull-out energy (W_p) were determined using Eqs. (1)–(3), respectively [58]:

$$\tau = \frac{P_B}{\pi d_f L_e} \tag{1}$$

$$G_d = \frac{2(P_A - P_B)^2}{\pi^2 E_f d_f^3} \tag{2}$$

$$W_p = \int_{\delta(P_B)}^{\delta(P_0)} P\, d\delta \tag{3}$$

where P_A corresponds to the peak force and P_B to the force at the initiation of the pull-out phase; d_f is the fiber diameter (Ref-PET – in Table 2); L_e is the embedded length of the fiber; E_f is the estimated Young's modulus (12.3 GPa) from single fiber tension tests on Ref-PET fibers; and, $\delta(P_B)$ and $\delta(P_0)$ are the displacements at pull-out initiation and completion (when the load reaches zero), respectively.

2.4.3. Compression test

To ascertain the strength evolution of the SH-LC^3-PET composites, compression tests were performed at various ages under investigation on cubes of size 40 mm. The cubes were retrieved from 160 mm long prismatic beams with 40 mm × 40 mm cross-sectional dimensions. The samples were pre-wetted and seal-cured in the climatic chamber until the designated testing date. A load-controlled regime with a rate of 2.4 kN/s was employed to determine the compressive strengths, with a minimum of six cubes tested at each age.

2.4.4. Uniaxial tension test

For uniaxial tension tests conducted on SH-LC^3-PET composites, specialized molds were employed to create dumbbell-shaped specimens, as depicted in Fig. 2. The use of this dumbbell shape was intended to ensure a gradual transition between the thicker loaded regions and the thinner gauge length, thereby minimizing stress concentrations. A layer-by-layer lamination technique was employed during the casting process to align the PET fibers parallel to the longitudinal (loading) direction. After allowing the specimens to cure for 24 hours within the molds, they were removed, adequately moistened, and promptly sealed for curing at specified ages within a climatic chamber. A few hours before testing, the sealed specimens were opened and marked with a fine stochastic pattern of black dots on a white surface, facilitating the application of digital image correlation (DIC) to detect crack initiation and propagation.

Two mechanical clamps were used to grip the dumbbell-shaped specimens in the Instron 8802 testing machine to grip the edge regions at the top and bottom of the specimens. This testing machine was equipped with a high-intensity light source and two cameras provided by GOM GmbH. The cameras were synchronized with the load sensor of the Instron machine, enabling automatic triggering of measurements when a force of 500 N was applied. Image capture during the test occurred at a sampling frequency of 2 Hz, while real-time force and machine displacement data were transferred to the ARAMIS professional software (GOM GmbH).

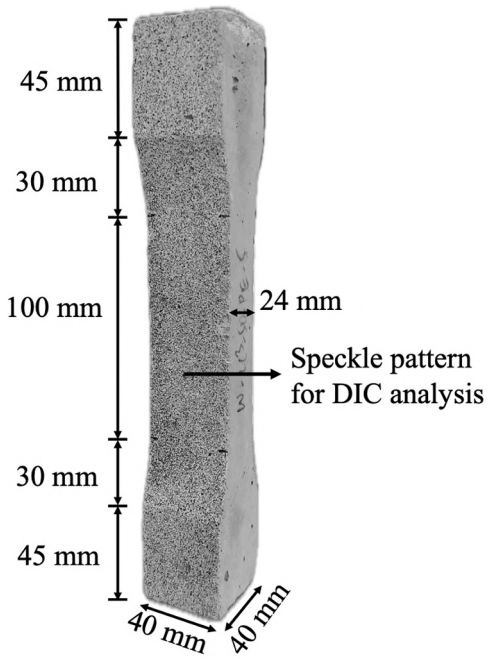

Fig. 2. Dumbbell-shaped specimen for uniaxial tension test equipped with speckle pattern.

To compute mean axial strains, two virtual strain gauges were constructed at the edges of the gauge length (located in the middle region measuring 100 mm long with a cross-section of 24 × 40 mm^2) using the reference picture taken before the initiation of the test. Subsequently, their relative deformations were measured in all subsequent images taken during the tests. Additionally, crack widths were determined by employing similar virtual calipers, and the number of cracks was manually counted.

3. Results and discussion

3.1. Single fiber tension test

Fig. 3 (a) shows the tensile stress-elongation curves of the reference PET fibers (Ref-PET), which exhibited linear elastic behavior between 0 and 80 MPa. This range of stresses was conventionally selected to estimate the initial modulus (E_1). The linear elastic phase of PET was terminated by a yield point [42,59,60], representing the transition from elastic to a pronounced plastic stage. During this phase, PET initially stretches due to strain-induced crystallization (SIC) resulting from the reorientation of spherulites parallel to the loading direction [61–63]. The secondary modulus (E_2) was determined after the completion of SIC, represented by a sharp increase in the tensile stress that occurred in the 300–500 MPa range.

The average tensile strength observed for the Ref-PET fibers was 584.8 MPa, which represents a remarkable decrease compared to the tensile strengths of the PVA and PE fibers studied in the previous study [20]. In fact, this reduction is approximately 2.7 times lower than the former and 4.3 times lower than the latter. This necessitates the design of a matrix compatible with the PET fibers' significantly lower mechanical properties and meets the required strength and energy criteria outlined in the context of micromechanics for SHCC [1].

The surfaces of the as-received PET fibers were subjected to SEM analysis, as depicted in Fig. 3 **(b)**. Conventionally, PET fibers present a smooth surface, as observed in other studies [37,42,64]. However, the

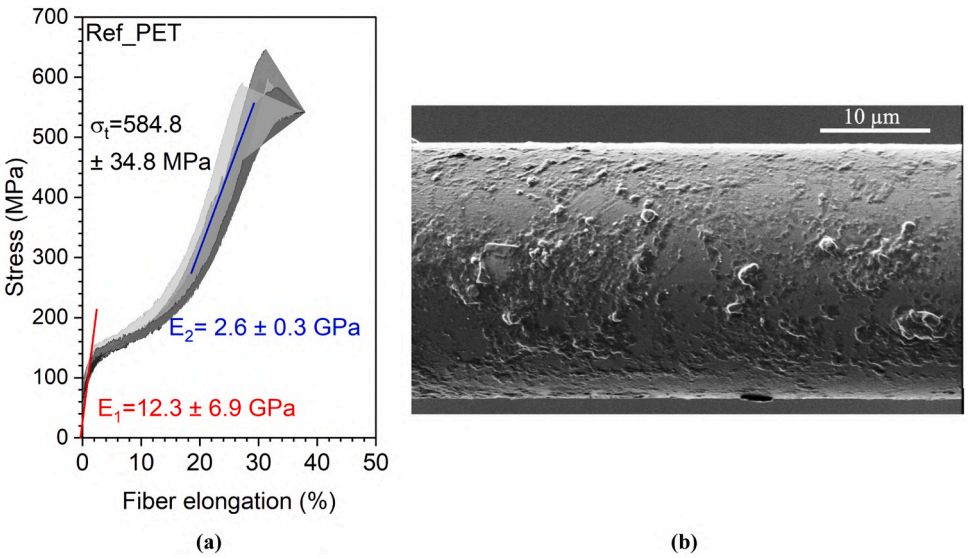

Fig. 3. (a) Stress *vs.* fiber elongation curves, and (b) SEM images showing the morphology of reference PET fibers. The enclosed gray-level gradients in the inlet (a) show the results' standard deviations.

PET fibers under scrutiny exhibited a marginally roughened surface. This surface texture offers a distinct advantage in enhancing friction during the extraction of fibers from cementitious matrices.

3.2. Out-of-matrix fiber aging – in the simulated pore solution

3.2.1. Physico-mechanical characterization via single fiber tension test

To quantify the degradation of PET fibers exposed to the simulated alkaline pore solution (pH=12.5), single-fiber tension tests and ESEM analysis were conducted on aged fibers, and the tensile strength values after different aging periods were compared with the reference values, see Fig. 4. In the tensile stress *vs.* fiber elongation curves of PET fibers after aging in pore solution for different time periods, the experimental variability is indicated by the enclosed colored area; additionally, $\sigma_{t,Ref}$ is highlighted, indicating the tensile strength of Ref_PET, *i.e.,* without fiber aging in alkaline solution.

No pronounced changes in the diameters of the fibers were discerned with aging in the simulated pore solution (Fig. 5 – gray line). In contrast, a distinct decrease in tensile strength was observed, indicating that the load-bearing capacity was strongly compromised. Indeed, after immersion for 7, 14, 28, and 60 days in pore solution, PET fibers underwent a 7.6 %, 11.7 %, 13.6 %, and 24.7 % decrease in tensile strength, respectively. This demonstrates the high susceptibility of these PET fibers to direct exposure to an alkaline environment, resulting in relatively rapid degradation.

Upon examining the surface of the exposed fibers (Fig. 4), no discernible signs of degradation are apparent within the first 28 days of exposure. However, beyond this age, the appearance of nano-craters (pitting) becomes evident, observable at the 60-day mark. This particular type of pitting serves as an indicative marker of alkaline hydrolysis affecting PET fibers, as previously noted in studies [37,40,65]. The underlying cause of this phenomenon can be attributed to various alkalis, such as Na, K, Li, Ca, and Mg, as well as the concentrations of hydroxides in the pore solution that build the pH levels [57]. Remarkably, the onset of pitting between 28 and 60 days coincides with the most substantial decline in load-bearing capacity. This correlation is linked to the role of these surface defects as stress concentrators, which result in localized high-stress levels, thereby initiating damage in these vicinities [66–70].

3.3. In-matrix fiber aging

3.3.1. Compression test

The compressive strengths of SH-LC^3-PET cubes were assessed at various curing ages, and the corresponding mean values are graphically presented in Fig. 6. At an early age of 7 days, the composite demonstrated strength of 17.1 MPa, which notably surged to 29.7 MPa after an additional 7 days of curing (*i.e.,* at 14 days), marking a substantial increase of 73.7 %. Beyond this threshold in curing time, there was no significant additional gain in strength. The measured strengths at 28 and 60 days exhibited only marginal increments of 1.3 % and 8.1 %, respectively, compared to the strength at 14 days.

This trend is consistent with the goal of achieving early stability in the matrix's mechanical strength. It indicates that most of the hydratable clinker phases and the pozzolan have nearly completed the reaction, with little or nothing left to hydrate and contribute further to the strength development. This means that no further matrix-induced changes in the fiber/matrix interface can be expected after 14 days of curing. This is a crucial aspect for low-strength and compliant PET fibers if strain hardening is to be achieved and maintained.

From a practical standpoint, the 28-day strength of SH-LC^3-PET, which stands at around 30–32 MPa, falls well within the range of 25–35 MPa concrete strength currently employed for many structural applications in developed countries [71].

In the early hydration stages, the development in the matrix's strength is ascribed to the "*filler effect*" brought about by low-grade calcined clay due to its high specific surface area [45]. In fact, SCMs generally exert a dual influence on clinker hydration: firstly, by providing additional nucleation sites for cement to precipitate its hydrates, and secondly, by diluting the overall system with respect to cement clinker. In the latter case, an increase in the effective water/cement (w/c) ratio at a certain water/binder (w/b) ratio caused by the high cement substitution is achieved, leading to "*dilutive effects*" that facilitate the precipitation of clinker hydrates in the abundance of space, promoting the hydration degrees [45,72,73].

In a physical sense, a higher w/c ratio implies the presence of a significant amount of space for the precipitation of hydrates, either from clinker hydration or via the pozzolanic reaction of SCMs. As long as other factors that influence hydration, such as relative humidity and temperature, do not impose constraints, space availability within the microstructure dictates the pace of hydration reactions [74]. This is the rationale behind the observation: systems with low w/c ratios exhibit a

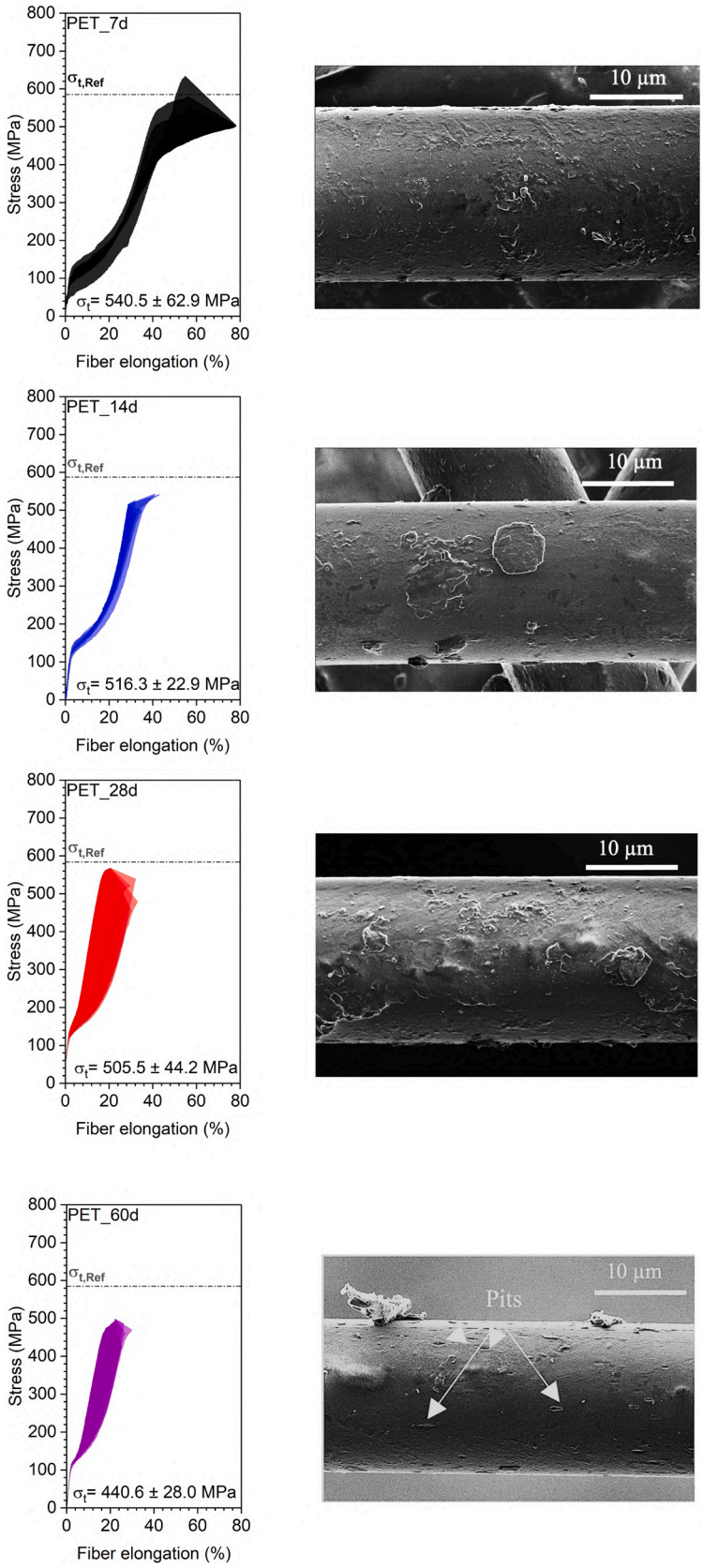

Fig. 4. Stress *vs.* fiber elongation curves of PET fiber exposed to pore solution for various ages (top to bottom on the left side: 7d, 14d, 28d, and 60d) and corresponding SEM images showing the surface morphology of these fibers on the right side.

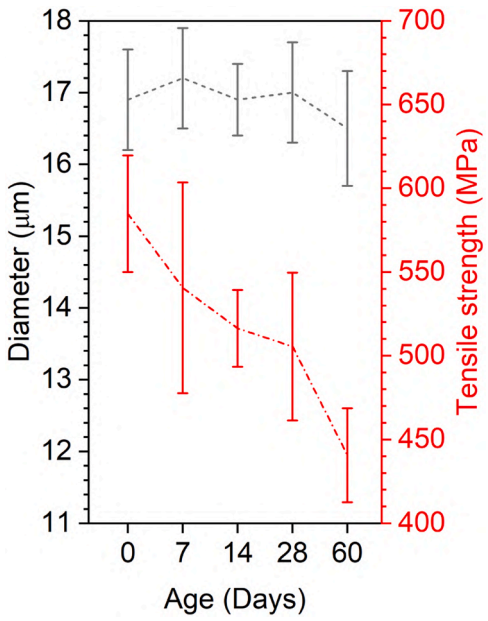

Fig. 5. The average diameter and tensile strength of PET fibers aged in simulated alkaline pore solution for 7, 14, 28, and 60 days. The reference PET fiber properties were plotted at 0 days.

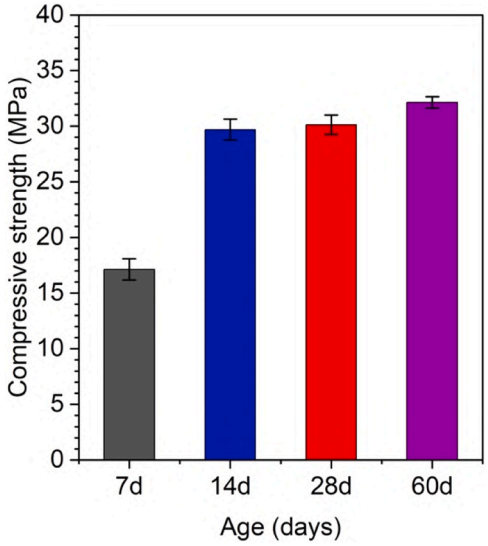

Fig. 6. Compressive strength of SH-LC^3-PET composites at various curing ages.

more compact microstructure after a certain curing period and do not attain complete clinker hydration degrees.

The effective w/c ratio in the investigated mixture (SH-LC^3) is about 1.60, a notably high value due to the excessive PC replacement. Observing the evolution of strength, it becomes apparent that most of the PC reacted within the initial 14 days of curing, resulting in a plateau in strength development over time. This aligns with the observations reported in reference [49], which documented complete clinker hydration in a highly diluted blended cement after 14 days, with no further enhancement of the pore structure.

Moreover, the pozzolanic properties of metakaolin, originating from calcined clay, and calcite, derived from limestone, in the mixture under investigation in this study facilitate the consumption of portlandite. Consequently, supplementary C-(A)-S-H and carboaluminate-AFm phases are formed [75]. Given the minimal gain in strength beyond 14 days, it is reasonable to infer that the time frame for the pozzolanic reaction is also mostly within the first two weeks of hydration age. The precipitated C-(A)-S-H from the pozzolanic reaction is typically characterized by a lower Ca/Si ratio with higher alkali binding capabilities, thereby buffering the alkalinity of the composite [57]. However, compression test results don't provide insights into the extent of degradation of the embedded PET fibers in the matrix. This crucial aspect will be addressed in the subsequent sections dealing with the single fiber pull-out and uniaxial tension tests, where the properties governing the fiber/matrix interface are explicitly assessed.

3.3.2. *Single fiber pull-out test*

The interfacial properties between the fibers and the matrix were determined through single-fiber pull-out tests. The force-displacement curves at different investigation time points are illustrated in the insets **(a-d)** of Fig. 7. The average curves for each time point, representing the mathematical mean of all pull-out curves within the shared displacement range of 0–6 mm, are presented in Fig. 7 **(e)**. This computation was conducted using the "*average multiple curves*" function available in OriginPro 2023b software developed by OriginLab Corp.

Most PET fibers exhibited a pull-out failure mode, characterized by an approximately linear decline in pull-out friction as the embedded PET fiber detaches from the SH-LC^3 matrix after the peak (load), as evident in Fig. 7. These findings align with the observations made by Lin *et al.* [42] regarding the pull-out behavior of both untreated and treated PET fibers within a cementitious matrix.

The strengthening/densification occurring at the interface between the fibers and the matrix correlates with the time-dependent development of compressive strength in the matrix, as discussed in Section 3.3.1. A more pronounced increase in the peak load was observed during the 7 and 14-day curing periods, which subsequently remained constant. Within this timeframe, the peak load nearly approached the values corresponding to the tensile strength of PET fibers, resulting in the rupture of some embedded PET fibers, particularly at the 14 and 28-day curing ages.

Furthermore, the smooth transition from peak load to the gradual pull-out phase, more prominent in 7 days results, was disrupted thereafter. In fact, in multiple samples cured for 14, 28, and 60 days, a sudden drop in load occurred after reaching the peak force, followed by the pull-out of the fibers from the surrounding matrix. This load drop phenomenon resembles the behavior typically observed during the pull-out of hydrophilic fibers, such as PVA, from cementitious matrices [76] – implying increased wettability (loss in hydrophobicity) of PET fibers, *i.e.,* formation of chemical bonding with the surrounding matrix.

Fig. 8 (a) illustrates the fraction of ruptured PET fibers in gray, while the percentage exhibiting a chemical bond with the SH-LC^3 matrix is depicted in red as a function of curing age. These fractions were calculated by dividing the number of samples displaying either of the two behaviors by the total number of single fiber pull-out tests conducted at that specific age. For instance, if 3 out of 10 single fiber pull-out tests displayed fiber rupture, and 5 displayed a load drop, then the percentages of ruptured fibers and those exhibiting chemical bonds are 30 % and 50 %, respectively. The remaining two samples exhibited the typical frictional pull-out behavior. To provide a visual representation of the load drops preceding the pull-out phase, Fig. 8 (b) presents a representative curve for each age.

The incidence of ruptured fibers increased as the curing age advanced, except for the samples cured for 60 days, which deviated from this pattern. Considering that the matrix properties remained stable after 14 days, this change in behavior at 60 days is most likely attributed only to PET fibers. The same trend was evident in the variations in load drop intensities, which also increased until the 28-day mark, followed by a subsequent decrease at 60 days (refer to Fig. 8 (b)). These observations suggest that the chemical bond between PET fibers and the SH-LC^3 matrix developed gradually over time. However, after a certain age, it started to diminish, resulting in the resurgence of the pull-out failure mode.

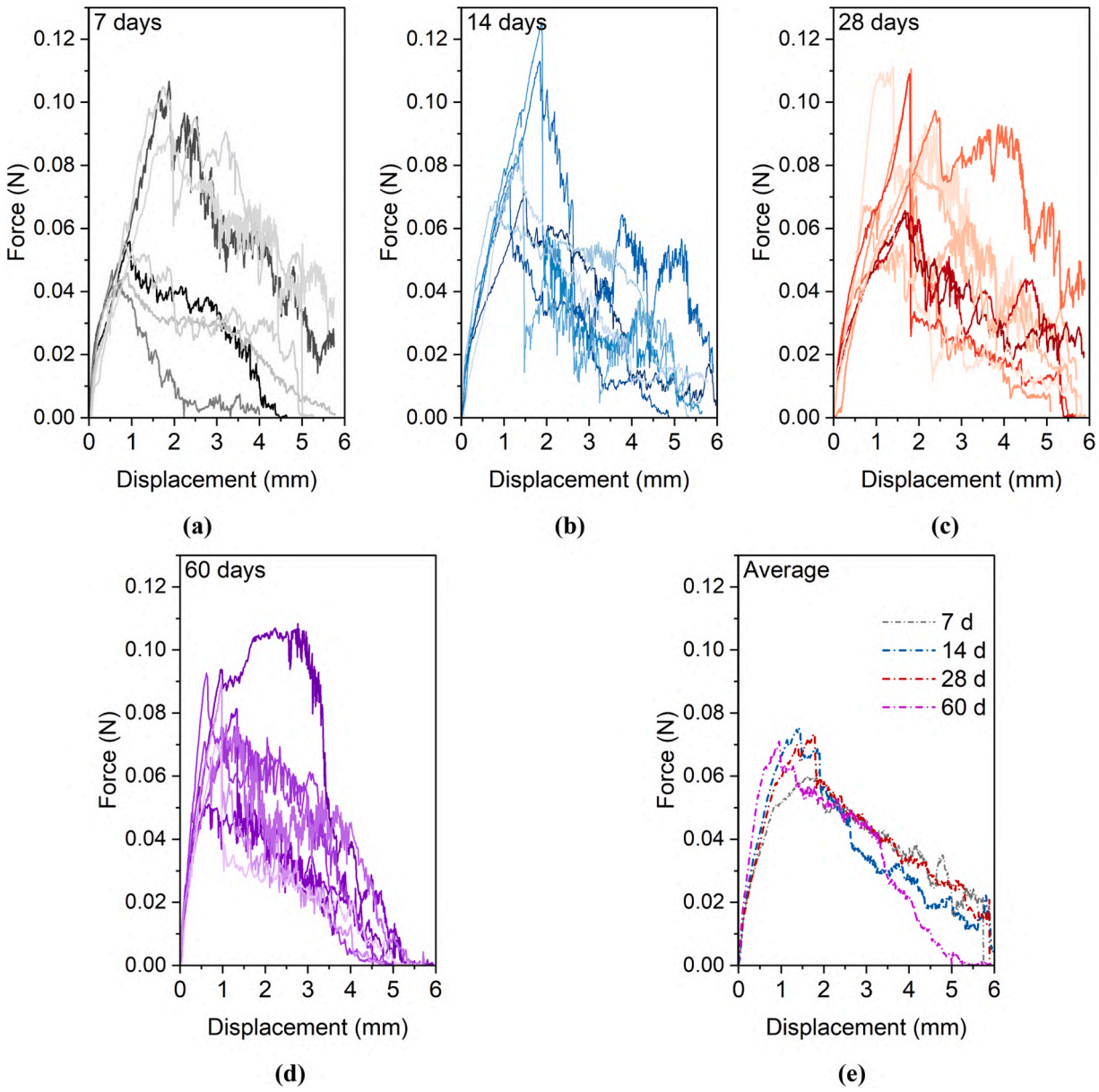

Fig. 7. Single fiber pull-out test results of SH-LC^3-PET: (a) at 7 days; (b) at 14 days; (c) at 28 days; (d) at 60 days; and (e) average curves at investigated ages.

Nonetheless, the proportion of fibers displaying this chemical bond in pull-out samples remained the same after 28 days, with approximately 50 % of samples exhibiting this load drop, while the remainder exhibited a smooth transition to the pull-out phase after debonding from the surrounding matrix.

One plausible explanation for the load drop observed in single-fiber pull-out curves is associated with prolonged embedding in a cementitious matrix. This extended exposure of PET to an alkaline environment results in slight improvements in water absorbency, manifested as a reduction in hydrophobicity due to alkaline hydrolysis, as documented in several prior studies [77–79]. It is anticipated that in SH-LC^3, the alkaline hydrolysis is restricted due to low clinker content but not completely absent. Additionally, portlandite crystals are released during the clinker hydration process and often accumulate near the fiber/-matrix interface [80]. Apart from the notching effects of these brittle wedged crystals, which can physically damage the fibers [38,81], perhaps partly contributing to fiber rupture at 14 and 28 days, these crystals also exhibit a lower surface area compared to the amorphous C-(A)-S-H, which possesses an open structure [82]. Therefore, as hydration progresses, the portlandite crystals near the fiber/matrix interface are consumed by metakaolin in calcined clay. This forms a dense stratum of C-(A)-S-H gel around the fiber, enhancing its contact with the fibers. This improved fiber/matrix interaction can be attributed, in part, to the open structure of C-(A)-S-H near the fiber vicinity and, in part, to the reduced hydrophobicity of PET. Furthermore, the interlocking between C-(A)-S-H and PET fibers might be promoted due to the notches caused by portlandite and the pitting sites on the surface of the PET fibers resulting from restricted alkaline hydrolysis.

To gain a deeper insight into the phenomenon leading to the peculiar behavior at 60 days of curing, ESEM analysis was performed on the extracted PET fibers (Fig. 9). From the ESEM micrographs, it can be seen that the scratches on the PET surface were more pronounced at 7 and 14 days, which can be attributed to the significant notching effect of portlandite. In addition, if the (restricted) in-matrix hydrolysis of PET fibers is indeed taking place, which may have, at first, improved their bonding with the surrounding C-(A)-S-H – the dominant phase in SH-LC^3 [45] – may later reduce PET's diameter, another consequence of alkaline hydrolysis, as observed from direct immersion in the pore solution.

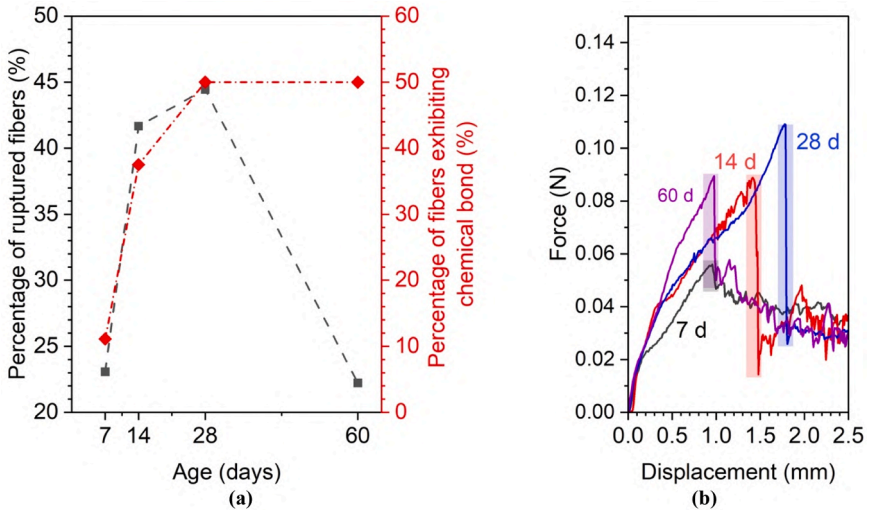

Fig. 8. (a) Percentage of ruptured PET fibers (in gray) and fibers showing a sudden drop in load before the pull-out phase (in red), and (b) representative curves showing load drop (highlighted region) in a single fiber pull-out test at various ages.

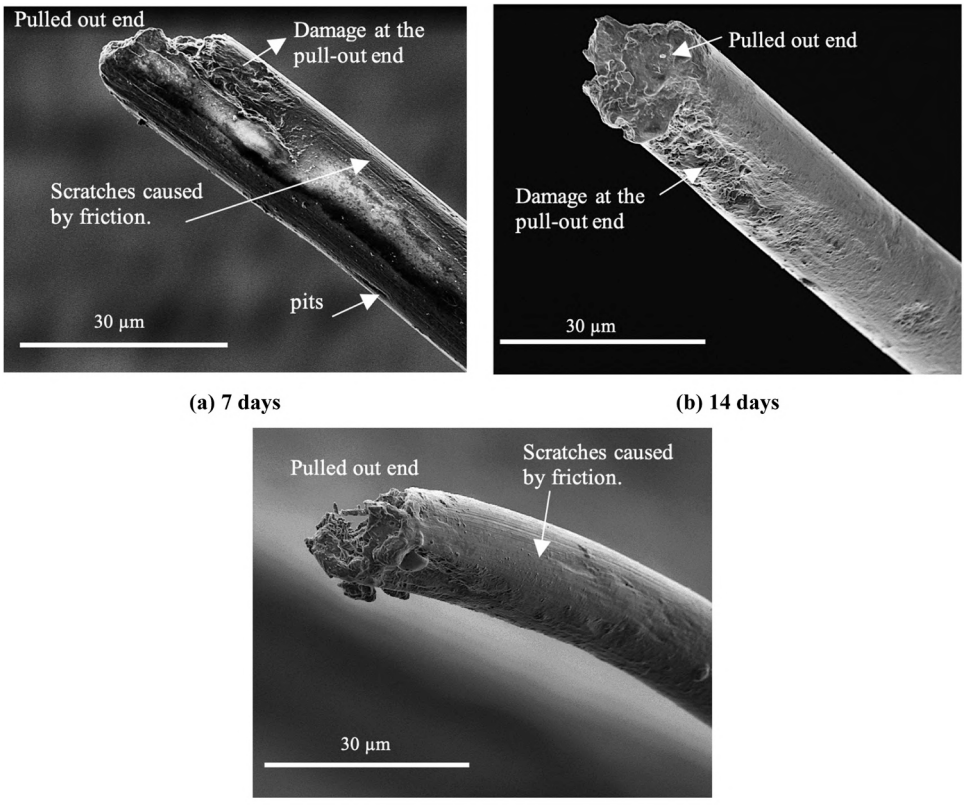

Fig. 9. SEM micrographs of pulled-out PET fibers after various curing ages.

Therefore, a reduction in the diameter of PET, resulting in some loss of contact with the surrounding matrix, may be the reason for the reduction in chemical bonding at 60 days. However, this diameter loss of the pulled-out PET fiber from SH-LC^3 could not be accurately calculated because the diameter can change due to PET stretching during pull-out under applied load. Nevertheless, further research focusing on in-depth investigations of the PET/SH-LC^3 interface is needed to understand and identify the mechanisms leading to the pull-out behavior observed in these investigations.

Table 4 summarizes the average values of the frictional bond strength, chemical bond strength, and pull-out energy calculated using Eqs. (1)–(3). As mentioned earlier, the reasons for the decrease in chemical bonding after 60 days of curing require further investigation. Still, the frictional bond strength and pull-out energy at 60 days shows comparable results to other curing ages. They mostly retain their pull-out behavior, stabilizing PET in the SH-LC^3 matrix's alkaline environment.

3.3.3. *Uniaxial tensile test*

Fig. 10 (a-d) displays the results of uniaxial tension tests conducted

Table 4
SH-LC^3-PET fiber/matrix frictional bonding properties. The standard deviations are mentioned in parentheses.

SH-LC^3-PET/Age	7 days	14 days	28 days	60 days
Average frictional bond strength, τ [MPa]	0.26 (0.14)	0.29 (0.11)	0.28 (0.10)	0.26 (0.09)
Average chemical bond strength, G_d [J/m^2]	0.11 (-)	3.52 (3.73)	4.43 (4.47)	1.16 (0.57)
Pull-out energy, W_p [J]	1.7×10^{-4}	1.5×10^{-4}	1.9×10^{-4}	1.5×10^{-4}

on the SH-LC^3-PET composites at the various investigated ages. The early segment of the curve, particularly useful for visualizing the first crack stress and the tensile Young's modulus, is presented on the left-hand side. Meanwhile, the complete tensile stress *vs.* strain response alongside average crack width curves are depicted in the middle. The crack patterns, determined through DIC analysis at three distinct strain levels, are provided on the right-hand side. The average values obtained from the uniaxial tension tests and the DIC crack analysis are summarized in Tables 5 and 6, respectively.

The SH-LC^3-PET composites displayed a notable strain-hardening behavior characterized by the occurrence of multiple crack formations following the first crack, indicated in cyan in Fig. 10 (e). Primarily, this first crack stress (σ_{fc}) is considered insensitive to the influence of fibers and is governed by the matrix cracking strength, defined by the pre-existing matrix flaws [83]. However, adding fibers to the matrix can influence the flaw distribution due to variations in the fiber volume content [83,84]. The linear elastic segment preceding the matrix cracking strength defines the matrix's stiffness, represented by Young's modulus (E), highlighted in yellow in Fig. 10 (e). With the progression in curing age, Young's modulus, matrix cracking strength, and tensile strength of the composites improved, particularly between 7 and 14 days. After 14 days of curing, the aforementioned properties stabilized, as evident in the results, *cf.* Table 5. This timeline pattern aligns with the

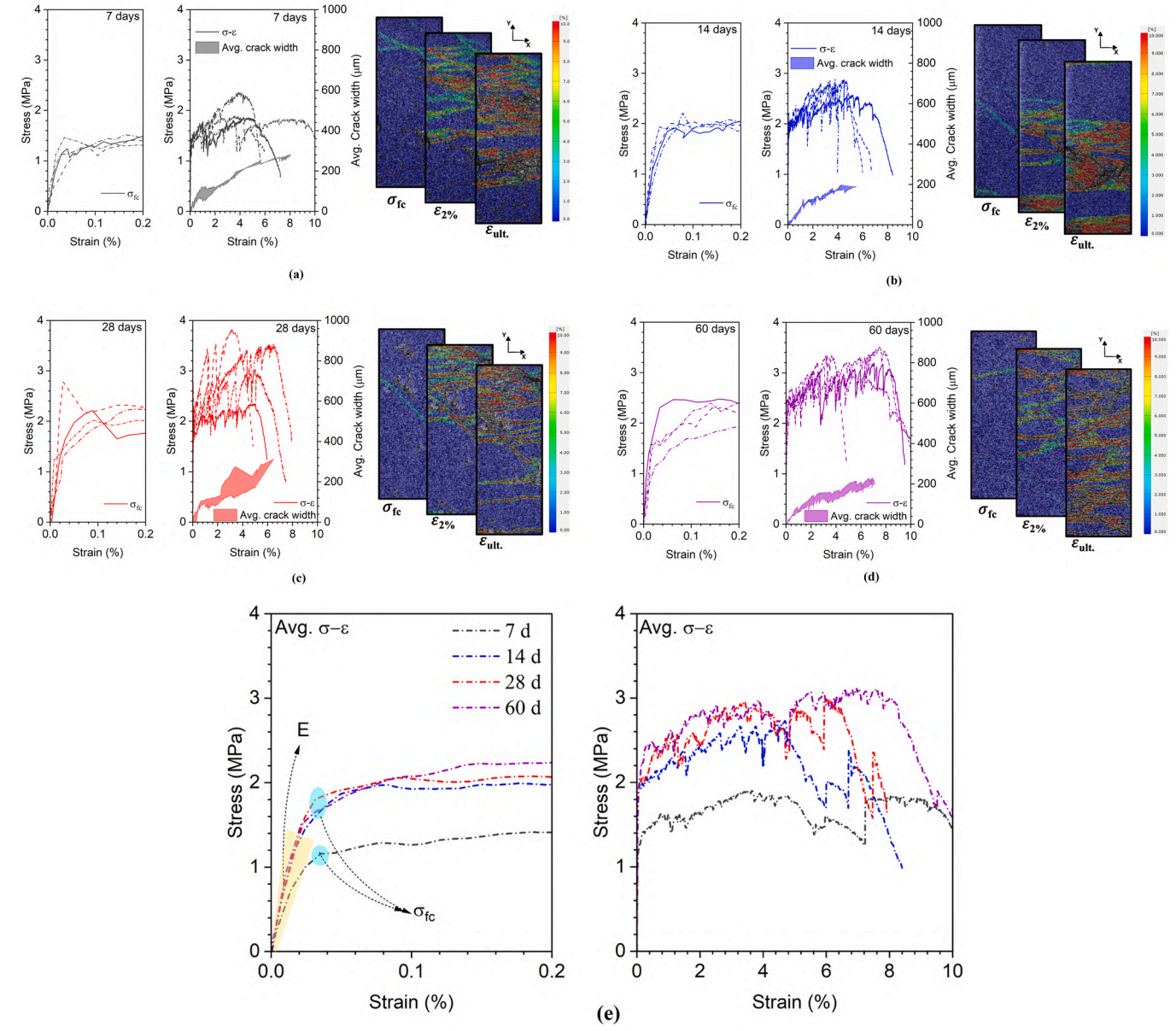

Fig. 10. Mechanical properties and DIC crack analysis of SH-LC^3-PET composites at various ages: (a) 7 days; (b) 14 days; (c) 28 days; and (d) 60 days. The data include σ-ε until 0.2 % strain to visualize the first crack stress (σ_{fc}) – left; complete σ-ε curves alongside average crack widths – middle; and DIC crack pattern at three specific points: σ_{fc}; 2 % tensile strain ($\varepsilon_{2\,\%}$); and ultimate strain (ε_{ult}) – right. The average stress *vs.* strain curves of SH-LC^3-PET at various investigated ages are shown in (e).

Table 5
Average values of various parameters from uniaxial tension test results of SH-LC^3-PET composites at different curing ages. The standard deviations are given in parentheses.

Composite	Age [days]	Young's modulus (E) - [GPa]	First crack stress (σ_{fc}) - [MPa]	Tensile strength ($\sigma_{ult.}$) - [MPa]	Ultimate strain ($\varepsilon_{ult.}$) - [%]	Work-to-fracture (W_f) - [kJ/m^3]
SH-LC^3-PET	7	4.3 (1.8)	1.4 (0.1)	2.0 (0.2)	5.0 (2.1)	82.0 (31.5)
	14	7.5 (2.3)	2.0 (0.1)	2.8 (0.1)	4.4 (0.6)	103.1 (13.1)
	28	9.3 (4.6)	2.3 (0.3)	3.2 (0.6)	4.8 (1.2)	125.6 (37.0)
	60	9.7 (2.6)	2.3 (0.2)	3.3 (0.2)	5.8 (2.0)	163.2 (60.6)

Table 6
DIC crack analysis of SH-LC^3-PET composites at various curing ages. The standard deviations are given in parentheses.

Composite	Age [days]	Avg. crack width @ $\varepsilon_{2\,\%}$ [μm]	Avg. crack width @ $\varepsilon_{ult.}$ [μm]	Max. crack width @ $\varepsilon_{ult.}$ [μm]	Crack density [/m]	Avg. crack spacing [mm]
SH-LC^3-PET	7	116.5 (8.8)	215.1 (59.6)	355.2 (104.8)	257.0 (35.0)	3.9 (0.6)
	14	114.7 (9.8)	192.7 (4.6)	301.8 (71.9)	247 (38.0)	4.1 (0.6)
	28	114.1 (21.3)	234.2.2 (70.5)	249.0 (56.8)	243 (42.0)	4.2 (0.7)
	60	115.0 (26.0)	213.4 (12.4)	309.2 (74.6)	297.0 (65.0)	3.5 (0.8)

observations made for the development of compressive strength and interfacial properties.

However, the distinctive feature of the SH-LC^3-PET composites lies in their tensile strain capacities, all of which exceeded 4 % at all examined ages. Specifically, at 7 days, the average ultimate strain recorded reached 5 %, while one of the specimens even exhibited an impressive strain capacity exceeding 8 %. Nevertheless, as the strength properties continued maturing beyond 7 days, a subtle decline in strain capacities became evident. For instance, at 14 and 28 days, the recorded mean strain capacities were 4.4 % and 4.8 %, respectively.

This change can be attributed to several factors. On the one hand, the matrix's strengthening due to the ongoing hydration process results in reduced porosity, progressively increasing the crack tip toughness. Consequently, this alteration slightly curtails the crack initiation and propagation potential. This trend is supported by the slight decrease in cracking densities at 14 and 28 days compared to the numbers recorded at 7 days, as specified in Table 6. On the other hand, the consolidation of the matrix, which simultaneously affects the fiber/matrix interfaces, leads to a higher likelihood of rupturing of bridging PET fibers. This claim aligns with the experimental evidence observed in the single-fiber pull-out tests, resulting in a reduction in complementary energy. Similar observations were pointed out and discussed by Wang and Li [85], linking the decrease in strain capacity of SHCC to the reduction in complementary energy and the increase in crack tip toughness of the matrix due to the curing process.

The recurring trend of SHCC diminishing strain capacities as the matrix's strength-related properties develop is well-documented in the literature. Additional confirmation of this phenomenon is available in studies that explore the influence of curing conditions marked by high relative humidity on SHCC. It is widely recognized that such conditions expedite the hydration process by supplying abundant moisture to anhydrous materials, thereby promoting the enhancement of strength and the densification of the matrix. This aspect is demonstrated in the investigations conducted by Zhu *et al.* [86], Xu *et al.* [87], Lu *et al.* [84], and Oh *et al.* [88].

However, just as the interfacial properties showed a peculiar behavior after 60 days of curing, a distinctive pattern also emerged for the SH-LC^3-PET composites after 60 days of hydration. Notably, despite Young's modulus and matrix strength showing no significant deviations compared to the samples cured for 28 days, the strain capacity of SH-LC^3-PET, instead of stabilizing or reducing, exhibited a remarkable increase, averaging 5.8 % (with two out of four specimens even exceeding 7 %). This is attributed to the fact that the tendency of the PET fibers to breakage almost diminishes, as observed in the single fiber pull-out tests, *cf.* Fig. 8 (a). Indeed, fiber pull-out becomes the dominant failure mode for the 60-day cured samples due to the significant reduction in chemical bonds compared to the 14- and 28-day cured counterparts. As a result, complementary energy increases, resulting in more widely distributed crack densities and reduced crack spacing, *cf.* Table 6. This phenomenon is also evident by observing the crack evolution at various strain levels in the DIC color maps at 60 days, as depicted in Fig. 10 (d), where the entire gauge length is saturated with multiple fine cracks.

Since the strain capacity of SHCC is mainly a function of the number of cracks formed in the gauge length and their widths, the elastic deformation of the matrix is negligible. These parameters strongly depend on the fiber/matrix interface bond. The maximum crack width in SHCC within the localization plane is the weakest section in the composite [89]. Fig. 11 plots the maximum crack width (at ultimate strain) against the chemical and mechanical bond strengths evaluated by single fiber pull-out tests. It can be seen that the lowest value of maximum crack width was observed for 28-day cured specimens, followed by the 14-day cured samples. The chemical and frictional bond strengths were the highest at these two curing ages. Therefore, the strain capacity of the SH-LC^3-PET is compromised as more fibers break in the localization plane due to the strong bond compared to the 7 or 60-day cured samples where the predominant fiber failure mode is pull-out. The maximum crack width of the 60-day cured specimens remains smaller than that of the 7-day cured specimens. However, they both generally exhibit similar frictional bond strength and pull-out fiber failure mode. The difference is in the chemical bond strength, which is higher in the 60-day cured samples. This results in a superior crack bridging capacity that efficiently redistributes the applied load back into the matrix, finally forming a more saturated crack pattern that improves its strain capacity than the 7-day cured samples.

Based on the experimental results of SH-LC^3-PET, the crack-bridging stress *vs.* single crack opening SHCC constitutive law was considered and plotted in Fig. 12. The first crack stress (σ_{fc}) was set equal to the matrix cracking strength obtained from the results of the uniaxial tensile test. The peak bridging strengths (σ_p) were equated to the tensile strengths of the SH-LC^3-PET. The data indicate that the pseudo-strain hardening (PSH) strength indices - σ_p/σ_{fc} ratios - at 7, 14, 28, and 60 days were 1.43, 1.40, 1.39, and 1.43, respectively. All PSH indices are higher than 1.2, which is typically regarded as satisfactory if strain-hardening behavior is to be expected [90].

Since the experiments were not performed on notched specimens, the constitutive laws were assumed for the energy criterion, *cf.* Fig. 12 (b). The crack opening displacements (δ) were taken to the crack within the localization plane, which showed the maximum crack width observed under the uniaxial tension test on SH-LC^3-PET. Since the predominant fiber failure mode in the 7- and 60-day cured specimens was pull-out, a gradually descending slope was considered in their softening branch as opposed to the more abrupt slope for the 14- and 28-day cured

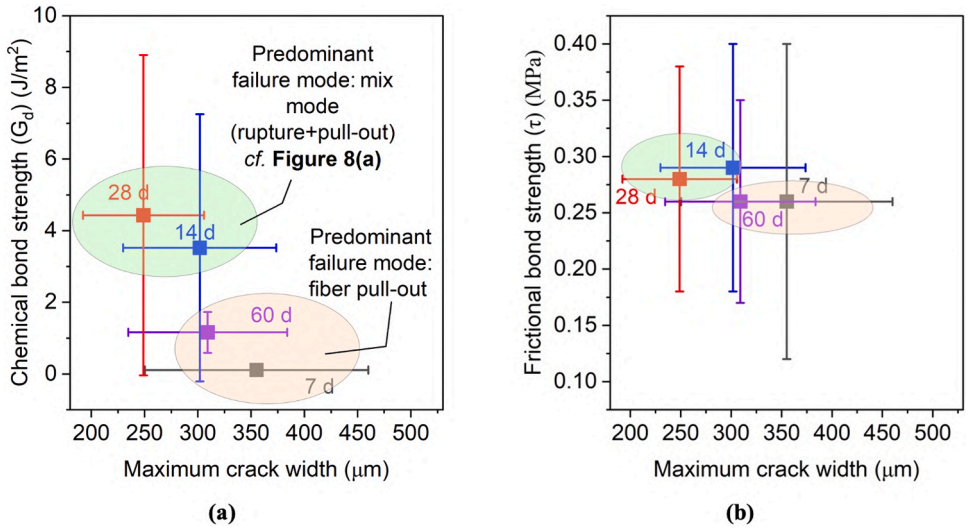

Fig. 11. Maximum crack widths at SHCC scale plotted against chemical (a) and frictional bond strengths (b) obtained via single fiber pull-out tests.

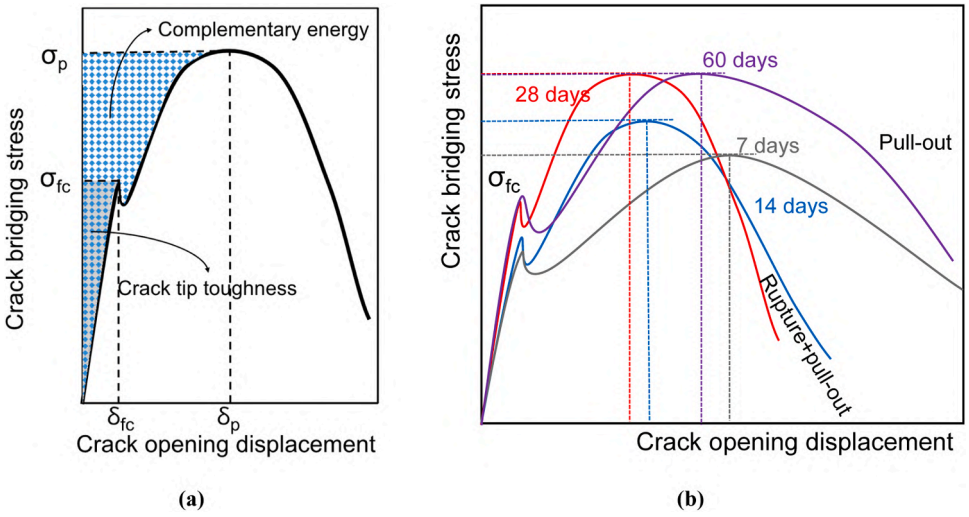

Fig. 12. SHCC constitutive law – crack-bridging stress *vs.* crack-opening displacement (a) and simulated constitutive law for SH-LC^3-PET at different curing ages based on tensile test and fiber pull-out results (b).

specimens. Similarly, the slope of the branch between first crack stress and peak bridging stress rises steeply for the 14- and 28-day cured specimens due to relatively stronger chemical bonds than their counterparts. From this schematic, it can be seen that the complementary energy for 7-day cured samples is mainly due to the poor frictional bond, which leads to the highest crack opening displacements, while for 14- and 28-day cured samples, although the crack bridging strengths have improved, the crack opening displacements are reduced due to the strong chemical bonds formed due to the limited alkaline hydrolysis of PET fibers. At 60 days, the chemical bonding is reduced to an extent that does not affect the crack bridging strength. Still, due to this reduction, the fiber failure mode changes from a mixed mode (rupture and pull-out) to a predominant pull-out mode, thereby increasing the crack opening displacements and thus improving the complementary energy. Future work will consider experiments on notched specimens to accurately assess the complementary energy (hatched area) and crack tip toughness (shaded area); see Fig. 12 (a).

Nonetheless, due to their remarkable ductility, the SH-LC^3-PET composites exhibit a high work-to-fracture, which is the area under the stress-strain curve until the onset of softening. This energy increases significantly with aging. Comparing the values observed at 7 days as a reference, the increase in work-to-fracture at 14 and 28 days are 27 % and 53 %, respectively, which are primarily attributed to the strength development of the composite. Despite preserving the matrix properties, the additional 30 % increase at 60 days compared to 28 days is due to the higher strain capacity resulting from the fiber/matrix interface changes.

An inherent limitation of SH-LC^3-PET composites is their limited control over crack width. Due to the compliant nature of PET fibers, which undergo significant yielding after a small amount of elastic deformation, there is a significant increase in the average crack width compared to SHCC reinforced with PE/PVA fibers. For example, the average crack width at ultimate strain for SH-LC^3-PET is almost twice that of SHCC with PE fibers [91,92] and four times that of PVA fibers [15,93,94]. It's important to note that wider cracks serve as pathways for the ingress of harmful substances, making the high crack widths in SH-LC^3-PET unfavorable for its durability [95]. Therefore, further optimization is needed to address this issue.

4. Conclusions

When dealing with cementitious composites reinforced with fibers

sensitive to alkaline environments, such as PET or glass fibers, it is advisable to thoroughly investigate the aging effects both within and outside the matrix. This study conducted a comprehensive experimental program to investigate these aspects and gain insight into virgin PET fibers' behavior. Micro- and meso-scale tests were performed, leading to the following conclusions:

- The PET fibers used in this study were highly sensitive to alkaline environments. After direct exposure to a simulated alkaline pore solution with a pH of 12.5 for 60 days, their load-bearing capacity was reduced by approximately 25 %. Examination through ESEM revealed widespread pitting on the fiber surface, resulting from alkaline hydrolysis.
- Intriguingly, single-fiber pull-out and uniaxial tensile tests demonstrated consistent mechanical performance of the same PET fibers for a duration of up to 60 days, which was the limit of investigation in this study. This consistency was observed when the fibers were embedded within a finely tailored cementitious matrix containing high volumes of limestone and calcined clay (comprising 75 % by weight of the binder). This underscores the significant role of SCMs in restricting or even preventing the deterioration of PET fibers.
- Prolonged curing of PET fibers within the SH-LC^3 matrix resulted in certain changes at the fiber/matrix interface, including the formation of a chemical bond with the surrounding matrix, which increased with curing age and was therefore attributed to (restricted) alkaline hydrolysis of PET. After 60 days of curing, the extent of chemical bonding decreased, which was attributed to a slight reduction in the diameter of the PET, another consequence of alkaline hydrolysis. However, these changes did not affect the frictional bond strength and pull-out energy. The underlying mechanisms responsible for these in-matrix transformations require further investigation.
- Due to the unique composition of the matrix (limited clinker proportion), SH-LC^3-PET's response in compression, single fiber pull-out, and uniaxial tensile tests showed almost all the strength and stiffness build-up in the early stages, between 14 and 28 days.
- The SH-LC^3-PET composites exhibited pronounced strain hardening behavior, with strain capacities exceeding 4 %. At the same time, the composites exhibited reasonable matrix and composite tensile strength at various ages. Notably, this remarkable strain-hardening behavior with as-received PET fibers in cementitious matrices appears unprecedented in the literature.
- The average crack widths obtained in this study were relatively higher than those typically observed in SHCC. This difference can be attributed to the substantial yielding of the PET fibers bridging the crack flanks and the relatively low fiber/matrix interfacial bonds leading to pullout, as dictated by micromechanical limitations on strain hardening behavior when using low strength and compliant fibers such as PET.

In brief, the SH-LC^3-PET composite developed in this study exhibits remarkable strain-hardening behavior and holds promising potential for more sustainable SHCC due to its significantly reduced Portland cement content. In addition, PET fibers are inexpensive and have a high recycling rate that can further improve PET-based products' economic and sustainability profile.

Future considerations and application areas

The poor crack width control of SH-LC^3-PET composites must be addressed for structural use under ordinary loading scenarios. Forthcoming investigations will entail the examination of less diluted mixtures containing SCMs, such as LC^3-50 and LC^3–35, as previously explored by the authors [45]. It is expected that in the case of these relatively high-strength matrices, the strain-hardening capabilities may diminish due to a narrower margin between the matrix strength and bridging fiber indices. Nevertheless, it remains essential to explore the extent to which enhanced strength and crack width control can be achieved and at what expense in terms of strain reduction. An accelerated carbonation curing process will be employed to mitigate the risk of alkaline hydrolysis affecting PET fibers within these matrices. This method can simultaneously reduce the alkalinity of the matrix and enhance the densification of the fiber/matrix interface [96]. If successful, these advancements will significantly expand the applicability of PET fibers in the context of SHCC. Furthermore, the hybridization of these PET fibers with short steel fibers [97] and continuous carbon textiles [18,98–100], including the novel mineral-impregnated yarns [101–106] in various LC^3 matrices, will also be explored in the future. These explorations aim to address the limitations associated with high crack widths and PET fibers' relatively low bridging strength.

With the current developments of SH-LC^3-PET, strengthening existing structures (protective overlays) against dynamic loading is a promising application. In this case, the inadequate crack width control becomes less of an issue. In fact, this composite is expected to perform well at high strain rates due to the pronounced plastic deformation of the PET fibers and the less dense matrix, which should be more strain rate sensitive than a stiff or high-strength matrix [5].

Funding

This work was supported by the German Research Foundation (Deutsche Forschungsgemeinschaft, DFG) [grant numbers 455631638, 287321140]

CRediT authorship contribution statement

Cesare Signorini: Writing – review & editing, Visualization, Supervision, Methodology, Conceptualization. **Ameer Hamza Ahmed:** Writing – review & editing, Writing – original draft, Visualization, Validation, Methodology, Investigation, Formal analysis, Data curation, Conceptualization. **Marco Liebscher:** Writing – review & editing, Visualization, Supervision, Project administration, Methodology, Funding acquisition, Formal analysis, Conceptualization. **Mariam Chikhradze:** Investigation, Data curation. **Viktor Mechtcherine:** Writing – review & editing, Supervision, Resources, Project administration, Funding acquisition. **Marko Butler:** Writing – review & editing, Supervision.

Declaration of Competing Interest

The authors declare that they have no known competing financial interests or personal relationships that could have appeared to influence the work reported in this paper.

Data Availability

Data will be made available on request.

Acknowledgements

The authors would like to thank ADVANSA GmbH (Hamm, Germany) for their technical support and provision of PET fibers.

References

[1] V. Li, From Micromechanics to structural engineering - the design of cementitious composites for civil engineering applications, J. Struct. Mech. Earthq. Eng. 10 (1992) 37–48.
[2] V.C. Li, On Engineered Cementitious Composites (ECC)- A Review of the Material and Its Applications, 1 (2003).
[3] V. Mechtcherine, O. Millon, M. Butler, K. Thoma, Mechanical behaviour of strain hardening cement-based composites under impact loading, Cem. Concr. Compos. 33 (2011) 1–11, https://doi.org/10.1016/j.cemconcomp.2010.09.018.

[4] I. Curosu, V. Mechtcherine, D. Forni, E. Cadoni, Performance of various strain-hardening cement-based composites (SHCC) subject to uniaxial impact tensile loading, Cem. Concr. Res. 102 (2017) 16–28, https://doi.org/10.1016/j.cemconres.2017.08.008.

[5] I. Curosu, V. Mechtcherine, O. Millon, Effect of fiber properties and matrix composition on the tensile behavior of strain-hardening cement-based composites (SHCCs) subject to impact loading, Cem. Concr. Res. 82 (2016) 23–35, https://doi.org/10.1016/j.cemconres.2015.12.008.

[6] Victor C. Li, Y. Leung Christopher K, Steady-state and multiple cracking of short random fiber composites, J. Eng. Mech. 118 (1992) 2246–2264, https://doi.org/10.1061/(ASCE)0733-9399(1992)118:11(2246).

[7] Y. Leung Christopher K, Design criteria for pseudoductile fiber-reinforced composites, J. Eng. Mech. 122 (1996) 10–18, https://doi.org/10.1061/(ASCE)0733-9399(1996)122:1(10).

[8] D. Zhang, J. Yu, H. Wu, B. Jaworska, B.R. Ellis, V.C. Li, Discontinuous micro-fibers as intrinsic reinforcement for ductile Engineered Cementitious Composites (ECC), Compos. Part B Eng. 184 (2020) 107741, https://doi.org/10.1016/j.compositesb.2020.107741.

[9] S. WangMicromechanics based matrix design for engineered cementitious composites, University of Michigan, 2005 .

[10] I. Curosu, M. Liebscher, V. Mechtcherine, C. Bellmann, S. Michel, Tensile behavior of high-strength strain-hardening cement-based composites (HS-SHCC) made with high-performance polyethylene, aramid and PBO fibers, Cem. Concr. Res. 98 (2017) 71–81, https://doi.org/10.1016/j.cemconres.2017.04.004.

[11] T. Gong, A.H. Ahmed, I. Curosu, V. Mechtcherine, On the synergetic action between strain-hardening cement based composites (SHCC) and carbon textile reinforcement under tensile loading. in: Proceedings of the 10th International Conference on Fracture Mechanics of Concrete and Concrete Structures, IA-FraMCoS, 2019, https://doi.org/10.21012/FC10.235471.

[12] I. Curosu, M. Liebscher, S. Burk, H. Li, S. Hempel, N. Raak, H. Rohm, V. Mechtcherine, Influence of fiber type on the tensile behavior of high-strength strain-hardening cement-based composites (SHCC) at elevated temperatures, Mater. Des. 198 (2021) 109397, https://doi.org/10.1016/j.matdes.2020.109397.

[13] Michael D. Lepech, Victor C. Li, Large-scale processing of engineered cementitious composites, MJ 105 (2008), https://doi.org/10.14359/19897.

[14] Michael D. Lepech, Victor C. Li, Richard E. Robertson, Gregory A. Keolelan, Design of green engineered cementitious composites for improved sustainability, MJ 105 (2008), https://doi.org/10.14359/20198.

[15] P. Jun, V. Mechtcherine, Behaviour of strain-hardening cement-based composites (SHCC) under monotonic and cyclic tensile loading, Cem. Concr. Compos. 32 (2010) 801–809, https://doi.org/10.1016/j.cemconcomp.2010.07.019.

[16] V. Mechtcherine, F.D.A. Silva, S. Müller, P. Jun, R.D.T. Filho, Coupled strain rate and temperature effects on the tensile behavior of strain-hardening cement-based composites (SHCC) with PVA fibers, Cem. Concr. Res. 42 (2012) 1417–1427, https://doi.org/10.1016/j.cemconres.2012.08.011.

[17] S. Müller, V. Mechtcherine, Use of strain-hardening cement-based composites (SHCC) for retrofitting, MATEC Web Conf. 199 (2018) 09006, https://doi.org/10.1051/matecconf/201819909006.

[18] T. Gong, A.H. Ahmed, I. Curosu, V. Mechtcherine, Tensile behavior of hybrid fiber reinforced composites made of strain-hardening cement-based composites (SHCC) and carbon textile, Constr. Build. Mater. 262 (2020) 120913, https://doi.org/10.1016/j.conbuildmat.2020.120913.

[19] I. Curosu, M. Liebscher, G. Alsous, E. Muja, H. Li, A. Drechsler, R. Frenzel, A. Synytska, V. Mechtcherine, Tailoring the crack-bridging behavior of strain-hardening cement-based composites (SHCC) by chemical surface modification of poly(vinyl alcohol) (PVA) fibers, Cem. Concr. Compos. 114 (2020) 103722, https://doi.org/10.1016/j.cemconcomp.2020.103722.

[20] I. Curosu, E. Muja, M. Ismailov, A.H. Ahmed, M. Liebscher, V. Mechtcherine, An experimental-analytical scale-linking study on the crack-bridging mechanisms in different types of SHCC in dependence on fiber orientation, Cem. Concr. Res. 152 (2022) 106650, https://doi.org/10.1016/j.cemconres.2021.106650.

[21] E.-H. Yang, V.C. Li, Strain-hardening fiber cement optimization and component tailoring by means of a micromechanical model, Constr. Build. Mater. 24 (2010) 130–139, https://doi.org/10.1016/j.conbuildmat.2007.05.014.

[22] Textile Exchange, Preferred fiber & Materials Market Report, 2022. https://textileexchange.org/app/uploads/2022/10/Textile-Exchange_PFMR_2022.pdf (accessed May 17, 2023).

[23] Advansa, P.E.T.Advansa, (n.d.). https://www.advansa.com/en/technical-applications/pet/ (accessed May 17, 2023).

[24] R. Rostami, M. Zarrebini, M. Mandegari, D. Mostofinejad, S.M. Abtahi, A review on performance of polyester fibers in alkaline and cementitious composites environments, Constr. Build. Mater. 241 (2020) 117998, https://doi.org/10.1016/j.conbuildmat.2020.117998.

[25] T. Ochi, S. Okubo, K. Fukui, Development of recycled PET fiber and its application as concrete-reinforcing fiber, Cem. Concr. Compos. 29 (2007) 448–455, https://doi.org/10.1016/j.cemconcomp.2007.02.002.

[26] S. Gupta, V.V.L.K. Rao, J. Sengupta, Evaluation of polyester fiber reinforced concrete for use in cement concrete pavement works, Road. Mater. Pavement Des. 9 (2008) 441–461, https://doi.org/10.1080/14680629.2008.9690127.

[27] U. Chaduvula, B.V.S. Viswanadham, J. Kodikara, A study on desiccation cracking behavior of polyester fiber-reinforced expansive clay, Appl. Clay Sci. 142 (2017) 163–172, https://doi.org/10.1016/j.clay.2017.02.008.

[28] D. Foti, Preliminary analysis of concrete reinforced with waste bottles PET fibers, Constr. Build. Mater. 25 (2011) 1906–1915, https://doi.org/10.1016/j.conbuildmat.2010.11.066.

[29] V. Corinaldesi, A. Nardinocchi, Influence of type of fibers on the properties of high performance cement-based composites, Constr. Build. Mater. 107 (2016) 321–331, https://doi.org/10.1016/j.conbuildmat.2016.01.024.

[30] J. Trejbal, L. Kopecký, P. Tesárek, J. Fládr, J. Antoš, M. Somr, V. Nežerka, Impact of surface plasma treatment on the performance of PET fiber reinforcement in cementitious composites, Cem. Concr. Res. 89 (2016) 276–287, https://doi.org/10.1016/j.cemconres.2016.08.018.

[31] A.H. Alani, N.M. Bunnori, A.T. Noaman, T.A. Majid, Durability performance of a novel ultra-high-performance PET green concrete (UHPPGC), Constr. Build. Mater. 209 (2019) 395–405, https://doi.org/10.1016/j.conbuildmat.2019.03.088.

[32] C. Signorini, V. Volpini, Mechanical performance of fiber reinforced cement composites including fully-recycled plastic fibers, Fibers 9 (2021) 16, https://doi.org/10.3390/fib9030016.

[33] C. Signorini, A. Nobili, Durability of fibre-reinforced cementitious composites (FRCC) including recycled synthetic fibres and rubber aggregates, Appl. Eng. Sci. 9 (2022) 100077, https://doi.org/10.1016/j.apples.2021.100077.

[34] M. Benzerara, Y. Biskri, M. Saidani, F. Slimani, R. Belouettar, High-temperature behavior of polyethylene-terephthalate-fiber-reinforced sand concrete: experimental investigation, Fibers 11 (2023) 46, https://doi.org/10.3390/fib11050046.

[35] Y. Wang, S. Backer, V.C. Li, An experimental study of synthetic fibre reinforced cementitious composites, J. Mater. Sci. 22 (1987) 4281–4291, https://doi.org/10.1007/BF01132019.

[36] J.-P. Won, C.-I. Jang, S.-W. Lee, S.-J. Lee, H.-Y. Kim, Long-term performance of recycled PET fibre-reinforced cement composites, Constr. Build. Mater. 24 (2010) 660–665, https://doi.org/10.1016/j.conbuildmat.2009.11.003.

[37] D.A. Silva, A.M. Betioli, P.J.P. Gleize, H.R. Roman, L.A. Gómez, J.L.D. Ribeiro, Degradation of recycled PET fibers in Portland cement-based materials, Cem. Concr. Res. 35 (2005) 1741–1746, https://doi.org/10.1016/j.cemconres.2004.10.040.

[38] M.E. Fernández, J. Payá, M.V. Borrachero, L. Soriano, A. Mellado, J. Monzó, Degradation PRocess of Postconsumer Waste Bottle Fibers Used in Portland Cement–based Composites, J. Mater. Civ. Eng. 29 (2017) 04017183, https://doi.org/10.1061/(ASCE)MT.1943-5533.0002007.

[39] R. Rostami, M. Zarrebini, M. Mandegari, K. Sanginabadi, D. Mostofinejad, S. M. Abtahi, The effect of concrete alkalinity on behavior of reinforcing polyester and polypropylene fibers with similar properties, Cem. Concr. Compos. 97 (2019) 118–124, https://doi.org/10.1016/j.cemconcomp.2018.12.012.

[40] M.S. Han, Y. Park, C.H. Park, Development of superhydrophobic polyester fabrics using alkaline hydrolysis and coating with fluorinated polymers, Fibers Polym. 17 (2016) 241–247, https://doi.org/10.1007/s12221-016-5693-7.

[41] J. Yu, J. Yao, X. Lin, H. Li, J.Y.K. Lam, C.K.Y. Leung, I.M.L. Sham, K. Shih, Tensile performance of sustainable strain-hardening cementitious composites with hybrid PVA and recycled PET fibers, Cem. Concr. Res. 107 (2018) 110–123, https://doi.org/10.1016/j.cemconres.2018.02.013.

[42] X. Lin, J. Yu, H. Li, J.Y.K. Lam, K. Shih, I.M.L. Sham, C.K.Y. Leung, Recycling polyethylene terephthalate wastes as short fibers in strain-hardening cementitious composites (SHCC), J. Hazard. Mater. 357 (2018) 40–52, https://doi.org/10.1016/j.jhazmat.2018.05.046.

[43] C. Lu, P. She, H. Chu, Y. Yao, C.K.Y. Leung, An investigation on the performance enhancement and cost reduction of engineered cementitious composites developed with local PVA and PET fibers, J. Sustain. Cem. Based Mater. (2022) 1–13, https://doi.org/10.1080/21650373.2022.2152898.

[44] C. Lu, J. Yu, C.K.Y. Leung, Tensile performance and impact resistance of strain hardening cementitious composites (SHCC) with recycled fibers, Constr. Build. Mater. 171 (2018) 566–576, https://doi.org/10.1016/j.conbuildmat.2018.03.108.

[45] A.H. Ahmed, S. Nune, M. Liebscher, T. Köberle, A. Willomitzer, I. Noack, M. Butler, V. Mechtcherine, Exploring the role of dilutive effects on microstructural development and hydration kinetics of limestone calcined clay cement (LC3) made of low-grade raw materials, J. Clean. Prod. (2023) 139438, https://doi.org/10.1016/j.jclepro.2023.139438.

[46] N. Beuntner, Zur Eignung und Wirkungsweise calcinierter Tone als reaktive Bindemittel- komponente im Zement, Universität der Bundeswehr München, 2017. https://athene-forschung.rz.unibw-muenchen.de/doc/121217/121217.pdf (accessed April 13, 2023).

[47] L. Wang, N. Ur Rehman, I. Curosu, Z. Zhu, M.A.B. Beigh, M. Liebscher, L. Chen, D. C.W. Tsang, S. Hempel, V. Mechtcherine, On the use of limestone calcined clay cement (LC3) in high-strength strain-hardening cement-based composites (HS-SHCC), Cem. Concr. Res. 144 (2021) 106421, https://doi.org/10.1016/j.cemconres.2021.106421.

[48] L. Wang, Z. Zhu, A. Hamza Ahmed, M. Liebscher, X. Zhu, V. Mechtcherine, Self-healing behavior of high-strength strain-hardening cement-based composites (HS-SHCC) blended with limestone calcined clay cement (LC3), Constr. Build. Mater. 370 (2023) 130633, https://doi.org/10.1016/j.conbuildmat.2023.130633.

[49] E. Berodier, K. Scrivener, Evolution of pore structure in blended systems, Cem. Concr. Res. 73 (2015) 25–35, https://doi.org/10.1016/j.cemconres.2015.02.025.

[50] B. Lothenbach, K. Scrivener, R.D. Hooton, Supplementary cementitious materials, Cem. Concr. Res. 41 (2011) 1244–1256, https://doi.org/10.1016/j.cemconres.2010.12.001.

[51] Y. Li, J. Li, E.-H. Yang, X. Guan, Mechanism study of crack propagation in river sand Engineered Cementitious Composites (ECC), Cem. Concr. Compos. 128 (2022) 104434, https://doi.org/10.1016/j.cemconcomp.2022.104434.

[52] A. Goldschmidt, About the hydration theory and the composition of the liquid phase of portland cement, Cem. Concr. Res. 12 (1982) 743–746, https://doi.org/10.1016/0008-8846(82)90037-0.
[53] E.M. Gartner, F.J. Tang, S.J. Weiss, Saturation factors for calcium hydroxide and calcium sulfates in fresh portland cement pastes, J. Am. Ceram. Soc. 68 (1985) 667–673, https://doi.org/10.1111/j.1151-2916.1985.tb10122.x.
[54] R.S. Barneyback, S. Diamond, Expression and analysis of pore fluids from hardened cement pastes and mortars, Cem. Concr. Res. 11 (1981) 279–285, https://doi.org/10.1016/0008-8846(81)90069-7.
[55] S. Diamond, Effects of two Danish flyashes on alkali contents of pore solutions of cement-flyash pastes, Cem. Concr. Res. 11 (1981) 383–394, https://doi.org/10.1016/0008-8846(81)90110-1.
[56] B. Lothenbach, Thermodynamic equilibrium calculations in cementitious systems, Mater. Struct. 43 (2010) 1413–1433, https://doi.org/10.1617/s11527-010-9592-x.
[57] A. Vollpracht, B. Lothenbach, R. Snellings, J. Haufe, The pore solution of blended cements: a review, Mater. Struct. 49 (2016) 3341–3367, https://doi.org/10.1617/s11527-015-0724-1.
[58] Z. Lin, T. Kanda, V.C. Li, On Interface Property Characterization and Performance of Fiber Reinforced Cementitious Composites, (1999). http://deepblue.lib.umich.edu/handle/2027.42/84718 (accessed July 23, 2023).
[59] J.-J. Zeng, Y.-Y. Ye, W.-Y. Gao, S.T. Smith, Y.-C. Guo, Stress-strain behavior of polyethylene terephthalate fiber-reinforced polymer-confined normal-, high- and ultra high-strength concrete, J. Build. Eng. 30 (2020) 101243, https://doi.org/10.1016/j.jobe.2020.101243.
[60] J.-J. Zeng, Y. Zhuge, S.-D. Liang, Y.-L. Bai, J. Liao, L. Zhang, Durability assessment of PEN/PET FRP composites based on accelerated aging in alkaline solution/seawater with different temperatures, Constr. Build. Mater. 327 (2022) 126992, https://doi.org/10.1016/j.conbuildmat.2022.126992.
[61] G. Schuur, The autoorientation mechanism of crystallization, J. Polym. Sci. 50 (1961) 191–209, https://doi.org/10.1002/pol.1961.1205015321.
[62] S.A. Jabarin, Strain-induced crystallization of poly(ethylene terephthalate), Polym. Eng. Sci. 32 (1992) 1341–1349, https://doi.org/10.1002/pen.760321802.
[63] M. Girard, C. Combeaud, N. Billon, Effects of annealing prior to stretching on strain induced crystallization of polyethylene terephthalate, Polymer 230 (2021) 124078, https://doi.org/10.1016/j.polymer.2021.124078.
[64] A. Bashiri Rezaie, M. Montazer, One-step preparation of magnetically responsive nano CuFe2O4/fatty acids/polyester composite for dynamic thermal energy management applications, Renew. Energy 143 (2019) 1839–1851, https://doi.org/10.1016/j.renene.2019.05.132.
[65] M.S. Ellison, L.D. Fisher, K.W. Alger, S.H. Zeronian, Physical properties of polyester fibers degraded by aminolysis and by alkalin hydrolysis, J. Appl. Polym. Sci. 27 (1982) 247–257, https://doi.org/10.1002/app.1982.070270126.
[66] T. Brückner, A. Eberl, S. Heumann, M. Rabe, G. Guebitz, Enzymatic and chemical hydrolysis of poly(ethylene terephthalate) fabrics, J. Polym. Sci. Part A Polym. Chem. 46 (2008) 6435–6443, https://doi.org/10.1002/pola.22952.
[67] F. Liu, X. Cui, S. Yu, Z. Li, X. Ge, Hydrolysis reaction of poly(ethylene terephthalate) using ionic liquids as solvent and catalyst, J. Appl. Polym. Sci. 114 (2009) 3561–3565, https://doi.org/10.1002/app.30981.
[68] F. Mousazadegan, S. Saharkhiz, M. Maroufi, Weight reduction of microfibre polyester fabric and the effect on its physical and mechanical properties, J. Text. Inst. 101 (2010) 716–728, https://doi.org/10.1080/00405000902812685.
[69] Z. Ömeroğulları Basyigit, Effects of Chemical and Surface Modification on Mechanical and Chemical Properties of Polyester Fabrics, (2018) 1344–1353.
[70] I. Čorak, A. Tarbuk, D. Đorđević, K. Višić, L. Botteri, Sustainable alkaline hydrolysis of polyester fabric at low temperature, Mater. (Basel) 15 (2022) 1530, https://doi.org/10.3390/ma15041530.
[71] P.-C. Aïtcin, Cements of yesterday and today: concrete of tomorrow, Cem. Concr. Res. 30 (2000) 1349–1359, https://doi.org/10.1016/S0008-8846(00)00365-3.
[72] E. Berodier, K. Scrivener, Understanding the Filler effect on the nucleation and growth of C-S-H, J. Am. Ceram. Soc. 97 (2014) 3764–3773, https://doi.org/10.1111/jace.13177.
[73] E.M.J. BerodierImpact of the supplementary cementitious materials on the kinetics and microstructural development of cement hydration, 2015.
[74] K.L. Scrivener, A. Nonat, Hydration of cementitious materials, present and future, Cem. Concr. Res. 41 (2011) 651–665, https://doi.org/10.1016/j.cemconres.2011.03.026.
[75] M. Antoni, J. Rossen, F. Martirena, K. Scrivener, Cement substitution by a combination of metakaolin and limestone, Cem. Concr. Res. 42 (2012) 1579–1589, https://doi.org/10.1016/j.cemconres.2012.09.006.
[76] V. Li, H. Wu, Y.-W. Chan, Interface Property Tailoring for Pseudo Strain-Hardening Cementitious Composites, (2011). https://doi.org/10.1007/978-94-015-8563-7_18.
[77] E.M. Sanders, S.H. Zeronian, An analysis of the moisture-related properties of hydrolyzed polyester, J. Appl. Polym. Sci. 27 (1982) 4477–4491, https://doi.org/10.1002/app.1982.070271135.
[78] M. Getnet, R. Chavan, Catalyzation of alkaline hydrolysis of polyester by oxidizing agents for surface modification, Int. J. Sci. 22 (2015).
[79] I. Donelli, G. Freddi, V.A. Nierstrasz, P. Taddei, Surface structure and properties of poly-(ethylene terephthalate) hydrolyzed by alkali and cutinase, Polym. Degrad. Stab. 95 (2010) 1542–1550, https://doi.org/10.1016/j.polymdegradstab.2010.06.011.
[80] M. Butler, V. Mechtcherine, S. Hempel, Experimental investigations on the durability of fibre–matrix interfaces in textile-reinforced concrete, Cem. Concr. Compos. 31 (2009) 221–231, https://doi.org/10.1016/j.cemconcomp.2009.02.005.
[81] M. Butler, V. Mechtcherine, S. Hempel, Durability of textile reinforced concrete made with AR glass fibre: effect of the matrix composition, Mater. Struct. 43 (2010) 1351–1368, https://doi.org/10.1617/s11527-010-9586-8.
[82] P. Tennis, H. Jennings, A model for two types of calcium silicate hydrate in the microstructure of Portland cement pastes, Cem. Concr. Res. 30 (2000) 855–863, https://doi.org/10.1016/S0008-8846(00)00257-X.
[83] H.-C. Wu, V.C. Li, Stochastic process of multiple cracking in discontinuous random fiber reinforced brittle matrix composites, Int. J. Damage Mech. 4 (1995) 83–102, https://doi.org/10.1177/105678959500400105.
[84] C. Lu, V.C. Li, C.K.Y. Leung, Flaw characterization and correlation with cracking strength in Engineered Cementitious Composites (ECC), Cem. Concr. Res. 107 (2018) 64–74, https://doi.org/10.1016/j.cemconres.2018.02.024.
[85] S. Wang, V.C. Li, High-early-strength engineered cementitious composites, Acids Mater. J. (2006).
[86] Y. Zhu, Z. Zhang, Y. Yao, X. Guan, Y. Yang, Effect of water-curing time on the mechanical properties of engineered cementitious composites, J. Mater. Civ. Eng. 28 (2016) 04016123, https://doi.org/10.1061/(ASCE)MT.1943-5533.0001636.
[87] M. Xu, J. Yu, J. Zhou, Y. Bao, V.C. Li, Effect of curing relative humidity on mechanical properties of engineered cementitious composites at multiple scales, Constr. Build. Mater. 284 (2021) 122834, https://doi.org/10.1016/j.conbuildmat.2021.122834.
[88] T. Oh, M.-J. Kim, N. Banthia, D.-Y. Yoo, Influence of curing conditions on mechanical and microstructural properties of ultra-high-performance strain-hardening cementitious composites with strain capacity up to 17.3%, Dev. Built Environ. 14 (2023) 100150 https://doi.org/10.1016/j.dibe.2023.100150.
[89] C. Lu, C.K.Y. Leung, Effect of fiber content variation on the strength of the weakest section in strain hardening cementitious composites (SHCC), Constr. Build. Mater. 141 (2017) 253–258, https://doi.org/10.1016/j.conbuildmat.2017.03.020.
[90] T. KandaDesign of engineered cementitious composites for ductile seismic resistant elements, 1998.
[91] A.H. Ahmed, M. Liebscher, V. Mechtcherine, in: M. Kunieda, T. Kanakubo, T. Kanda, K. Kobayashi (Eds.), Mechanical Performance of Strain Hardening Limestone Calcined Clay Cementitious Composites (SHLC4) Subject to Wet-Dry Cycles, Strain Hardening Cementitious Composites, Springer International Publishing, Cham, 2023, pp. 3–12, https://doi.org/10.1007/978-3-031-15805-6_1.
[92] G. Gong, M. Guo, Y. Zhou, S. Zheng, B. Hu, Z. Zhu, Z. Huang, Multiscale investigation on the performance of engineered cementitious composites incorporating pe fiber and limstone calcined clay cement (LC3), Polymers 14 (2022) 1291, https://doi.org/10.3390/polym14071291.
[93] En-Hua Yang, Yingzi Yang, Victor C. Li, Use of high volumes of fly ash to improve ECC mechanical properties and material greenness, MJ 104 (2007), https://doi.org/10.14359/18966.
[94] D. Zhang, B. Jaworska, H. Zhu, K. Dahlquist, V.C. Li, Engineered cementitious composites (ECC) with limestone calcined clay cement (LC3), Cem. Concr. Compos. 114 (2020) 103766, https://doi.org/10.1016/j.cemconcomp.2020.103766.
[95] G.P.A.G. Van Zijl, V. Slowik, eds., A Framework for Durability Design with Strain-Hardening Cement-Based Composites (SHCC), Springer Netherlands, Dordrecht, 2017. https://doi.org/10.1007/978-94-024-1013-6.
[96] Z. Liu, W. Meng, Fundamental understanding of carbonation curing and durability of carbonation-cured cement-based composites: A review, J. CO2 Util. 44 (2021) 101428, https://doi.org/10.1016/j.jcou.2020.101428.
[97] B.T. Huang, J. Zhu, K.-F. Weng, V. Li, Ultra-high-strength engineered/strain-hardening cementitious composites (ECC/SHCC): material design and effect of fiber hybridization, Cem. Concr. Compos. 129 (2022) 104464, https://doi.org/10.1016/j.cemconcomp.2022.104464.
[98] R. Barhum, V. Mechtcherine, Influence of short dispersed and short integral glass fibres on the mechanical behaviour of textile-reinforced concrete, Mater. Struct. 46 (2013) 557–572, https://doi.org/10.1617/s11527-012-9913-3.
[99] R. Barhum, V. Mechtcherine, Effect of short, dispersed glass and carbon fibres on the behaviour of textile-reinforced concrete under tensile loading, Eng. Fract. Mech. 92 (2012) 56–71, https://doi.org/10.1016/j.engfracmech.2012.06.001.
[100] I. Curosu, A. Omara, A. Ahmed, V. Mechtcherine, Probabilistic finite element modeling of textile reinforced SHCC subjected to uniaxial tension, Materials 14 (2021) 3631, https://doi.org/10.3390/ma14133631.
[101] M. Liebscher, J. Zhao, G. Wilms, A. Michel, K. Wilhelm, V. Mechtcherine, Influence of roller configuration on the Fiber–Matrix distribution and mechanical properties of continuously produced, mineral-impregnated carbon fibers (MCFs), Fibers 10 (2022) 42, https://doi.org/10.3390/fib10050042.
[102] R. Silva, J. Zhao, M. Liebscher, I. Curosu, F. Silva, V. Mechtcherine, Bond behavior of polymer- and mineral-impregnated carbon fiber yarns towards concrete matrices at elevated temperature levels, Cem. Concr. Compos. 133 (2022) 104685, https://doi.org/10.1016/j.cemconcomp.2022.104685.
[103] J. Zhao, M. Liebscher, V. MechtcherineMineral-impregnated carbon-fiber (MCF) as novel alternative to fiber-reinforced polymer (frp) for reinforcing concrete and structural safety at elevated temperatures, 2023.
[104] J. Zhao, M. Liebscher, T. Köberle, A. Almanla, V. Mechtcherine, Mineral-impregnated carbon-fiber (MCF) composites made with differently sized fly-ash geopolymers for durable light weight and high temperature applications, Cem.

Concr. Compos. 138 (2023) 104950, https://doi.org/10.1016/j.cemconcomp.2023.104950.

[105] J. Zhao, A. Ahmed, M. Liebscher, A. Bartsch, E. Ivaniuk, M. Butler, V. Mechtcherine, Durable Textile-reinforced Concrete Made of Fast-setting, Mineralimpregnated Carbon-fibers (MCF) Reinforcements and Alkaline-activated Matrix, 2023. https://doi.org/10.23967/c.dbmc.2023.003.

[106] J. Zhao, A.H. Ahmed, M. Liebscher, A. Bartsch, E. Ivaniuk, M. Butler, J. Kohout, P. Hájková, V. Mechtcherine, Thermomechanical behavior of textile-reinforced geopolymer concrete based on mineral-impregnated carbon-fibers (MCFs) composites, Cem. Concr. Compos. 150 (2024) 105555, https://doi.org/10.1016/j.cemconcomp.2024.105555.